# The Presidents' Day Snowstorm of 18–19 February 1979: A Subsynoptic-Scale Event

LANCE F. BOSART[1]

*Department of Atmospheric Science, State University of New York at Albany, Albany, NY 12222*

(Manuscript received 4 September 1980, in final form 20 March 1981)

ABSTRACT

On 18–19 February 1979 a major east coast cyclone deposited a record-breaking snowfall on the Middle Atlantic States. The storm is noteworthy because of the failure of the operational prediction models to signal the intensity of the event. The life cycle of the cyclone is reviewed with emphasis on the synoptic and mesoscale features and their possible linkage.

Prior to cyclogenesis the synoptic pattern features a massive cold anticyclone near the Great Lakes with a broad baroclinic zone extending from Texas eastward to the Atlantic coast. A region of enhanced lower tropospheric baroclinicity develops along the Carolina coastal strip in response to significant oceanic sensible and latent heat fluxes which warm, moisten and destabilize the boundary layer. Cyclogenesis is initiated along the coastal front as the result of lower tropospheric warm advection. The importance of the coastal front is that it effectively steers the cyclone north-northeastward parallel to the coast such that it eventually acquires a favorable phase relationship for deepening with respect to a vigorous short-wave trough moving eastward from the Ohio Valley by 1200 GMT 19 February.

Explosive deepening takes place in the ensuing 6 h coincident with the outbreak of convection near the storm center. By 1800 GMT, satellite pictures reveal a closed, clear storm eye while surface ship and drilling rig data disclose the presence of minimal hurricane force winds, primarily in the northern semicircle of the storm. Unlike a hurricane, however, the convection is asymmetric with respect to the vortex, being concentrated in the region of strongest surface winds.

The major operational model errors stem from poor sea level pressure and quantitative precipitation prognoses. Evidence is presented that initial analysis deficiencies coupled with inadequate boundary-layer and convective precipitation physics precluded a successful model forecast in this case.

## 1. Introduction

This is a paper about the memorable snowstorm of 18–19 February 1979 in the Middle Atlantic States. Storm snowfalls totaled in the vicinity of 60 cm in portions of eastern Virginia, Maryland and Delaware with a number of localities reporting record 24 h snowfalls and total amount on the ground. Additional details and a description of the larger scale circulation regimes are found in Dickson (1979).

An equally interesting facet of this cyclonic event was the failure of the operational Limited Fine Mesh (LFM-II) and Seven-Layer Primitive Equation (7LPE) models in use at the National Meteorological Center (NMC) to adequately predict the cyclogenesis. Numerical weather prediction has made tremendous strides in the last 25 years, a point eloquently made by Reed (1977), and confirmed by the spectacular success of the LFM model in providing early warning of the famous Boston blizzard of February 1978 (Brown and Olson, 1978). Consequently, the failure of the LFM-II to predict major cyclogenesis over the conterminous United States and vicinity must be viewed as a rather rare event that is worthy of research.

Cyclogenesis was initiated along a Carolina coastal front of the type described by Bosart *et al.* (1972) and Bosart (1975). Cyclogenesis then proceeded at a more rapid rate in response to the approach of a short wave from the Ohio Valley. The explosive deepening phase of the cyclone coincided with the outbreak of convection near the storm center, a situation not unlike the development of a major oceanic cyclone which battered the *Queen Elizabeth II* in September 1978 as described by Gyakum (1980).[2]

This paper will describe the cyclone development in detail with emphasis on some important mesoscale features. Sections 2 and 3 contain a synoptic overview and quasi-geostrophic diagnosis, respectively. A mesoscale description of the coastal front is contained in Section 4 with supporting radar observations given in Section 5. Coastal frontogenesis is described in Section 6. Evidence for convective

[1]Work initiated while the author was on sabbatical leave at the Massachusetts Institute of Technology for the 1978–79 academic year.

[2] Gyakum, J. R., 1980: On the evolution of the QE II storm. *Preprints Eighth Conf. Weather Forecasting and Analysis*, Denver, Amer. Meteor. Soc., 23–28.

0027-0644/81/071542-25$10.25

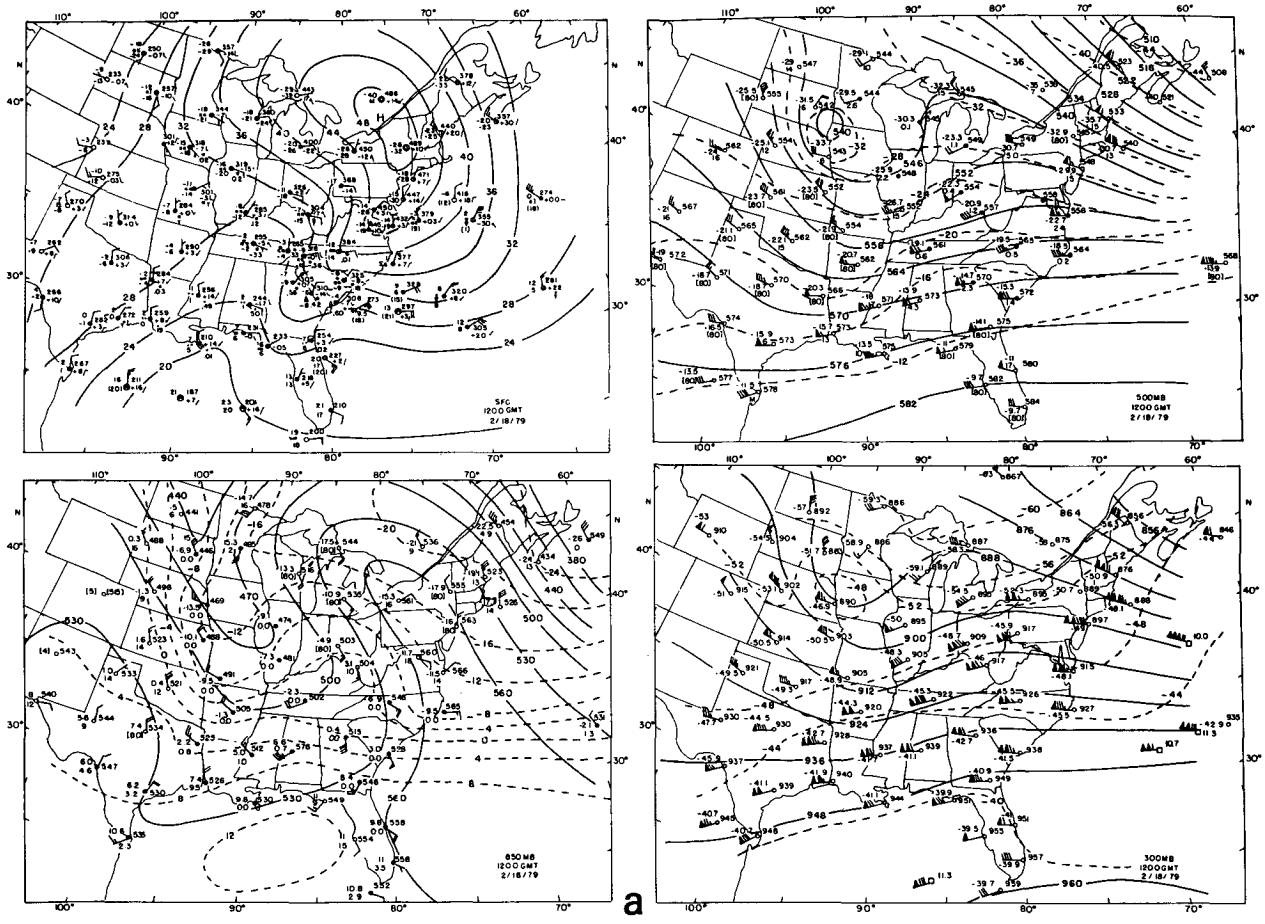


FIG. 1. Surface, 850, 500 and 300 mb maps for 1200, 0000 and 1200 GMT 18–19 February 1979. Conventional plotting and analysis scheme. Winds in m $s^{-1}$ [pennant = 25 m $s^{-1}$, full (half) barb = 5 (2.5) m $s^{-1}$], temperature in °C. Heights, surface pressures and isotherms indicated by solid and dashed lines, respectively. Solid station circles above the surface indicate a temperature-dew point temperature spread ≤ 5°C. Aircraft observations are entered on the 300 mb charts.

influences on cyclogenesis is documented in Section 7. Section 8 presents an analysis of aspects of the operational NMC LFM-II model failure for this case. A perspective view of the development appears in Section 9 with the conclusions given in Section 10.

## 2. Synoptic overview

The initial development of the Presidents' Day storm should be appreciated from the perspective of the winter of 1978–79. January was an extremely cold month over much of the interior of the conterminous United States (see, e.g., Wagner, 1979). Eastern New England was one of the few regions to experience a positive monthly temperature anomaly. Record and near-record monthly precipitation totals were posted in many northeastern locations in response to an active coastal zone storm track. Just prior to the end of January an abrupt circulation reversal occurred which ended the anomalously wet regime and ushered in a period of intense cold across the northeastern United States with little attendant precipitation. The height of the cold air outbreak was reached 17–18 February as a massive 1050 mb anticyclone invaded eastern North America. Following the Presidents' Day snowstorm another equally abrupt circulation reversal occurred which brought the return of warm and relatively wet conditions to much of the eastern United States. Within one week all traces of snow had disappeared from the Middle Atlantic States region.

A series of synoptic-scale surface, 850, 500 and 300 mb maps for 1200 GMT 18 February through 1200 GMT 19 February are presented in Fig. 1. At the beginning of the period the most impressive feature is the massive anticyclone centered over upper New York State. Cold air is entrenched from the western Atlantic to the Continental Divide. Of particular interest is the wedge of cold air to the east of the Appalachians which is reflected hydrostati-

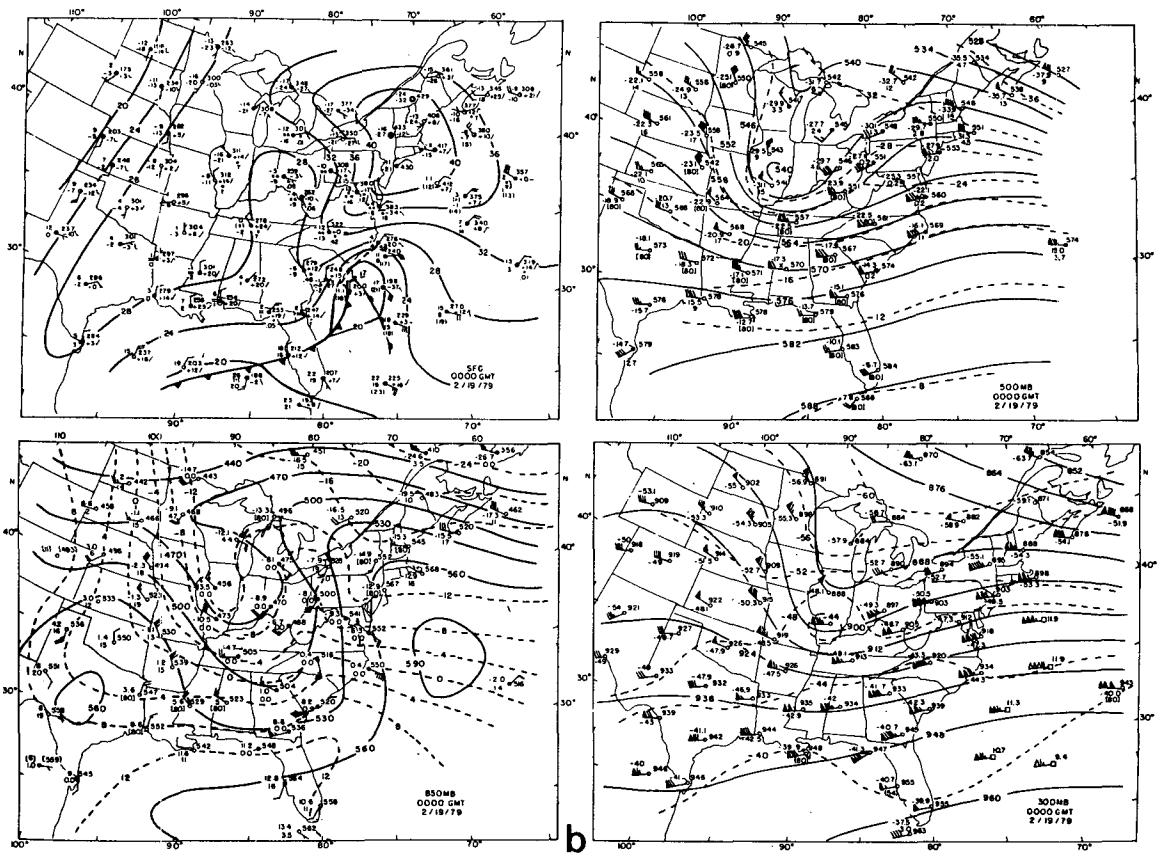


FIG. 1. (*Continued*)

cally in a surface pressure ridge. Weak troughs are located east of the Carolina coast and west of the Appalachians. Considerable precipitation is found across the southeastern United States in association with lower tropospheric warm advection that is readily seen on the 850 mb map.

Our period of interest begins *after* a swath of snow 15–25 cm deep has been deposited over portions of the southeastern United States north of a quasi-stationary baroclinic zone located across central Florida. This baroclinic zone was forced southward in the previous 24–36 h by the massive anticyclone moving eastward from the northern Great Lakes. Cyclogenesis, however, is initiated northeast of Florida. At no time is there any evidence for a cyclonic circulation moving eastward across Florida from the Gulf of Mexico. A major purpose of this paper is to provide some evidence of the important role of boundary-layer processes in determining where incipient development will occur within the broad synoptic-scale baroclinic zone.

At 850 mb the dominant feature is a strong baroclinic zone extending westward from Bermuda with exceptionally cold air over the ocean to the north. Pronounced warm advection is occurring along the Carolina coast with especially strong and ageostrophic winds seen at Charleston, South Carolina. (See Fig. 25 and the Appendix for information on specific locations mentioned in the test.) This ageostrophic flow pattern extends upward to 700 mb (not shown). In the mid and upper troposphere the most noteworthy feature is the *absence* of any significant 500 mb trough in the vicinity of the incipient Carolina coastal cyclonic circulation. The area of pronounced lower tropospheric warm advection in the Carolinas tends to lie beneath the right front exit portion of a 300 mb jet streak circulation centered over Tennessee. The entrance region of a downstream jet streak circulation is found over southeastern New England.

By 0000 GMT 19 February a definite cylonic circulation is seen east of Charleston, with a strong easterly geostrophic flow to the north. Warm advection remains dominant in the lower tropospheric storm environment. At 500 mb the trough previously centered over northwestern Iowa is now located in east central Illinois. The central trough height value has not changed in 12 h although the half-wavelength between the trough and the downstream ridge has shortened. Significant troughing is

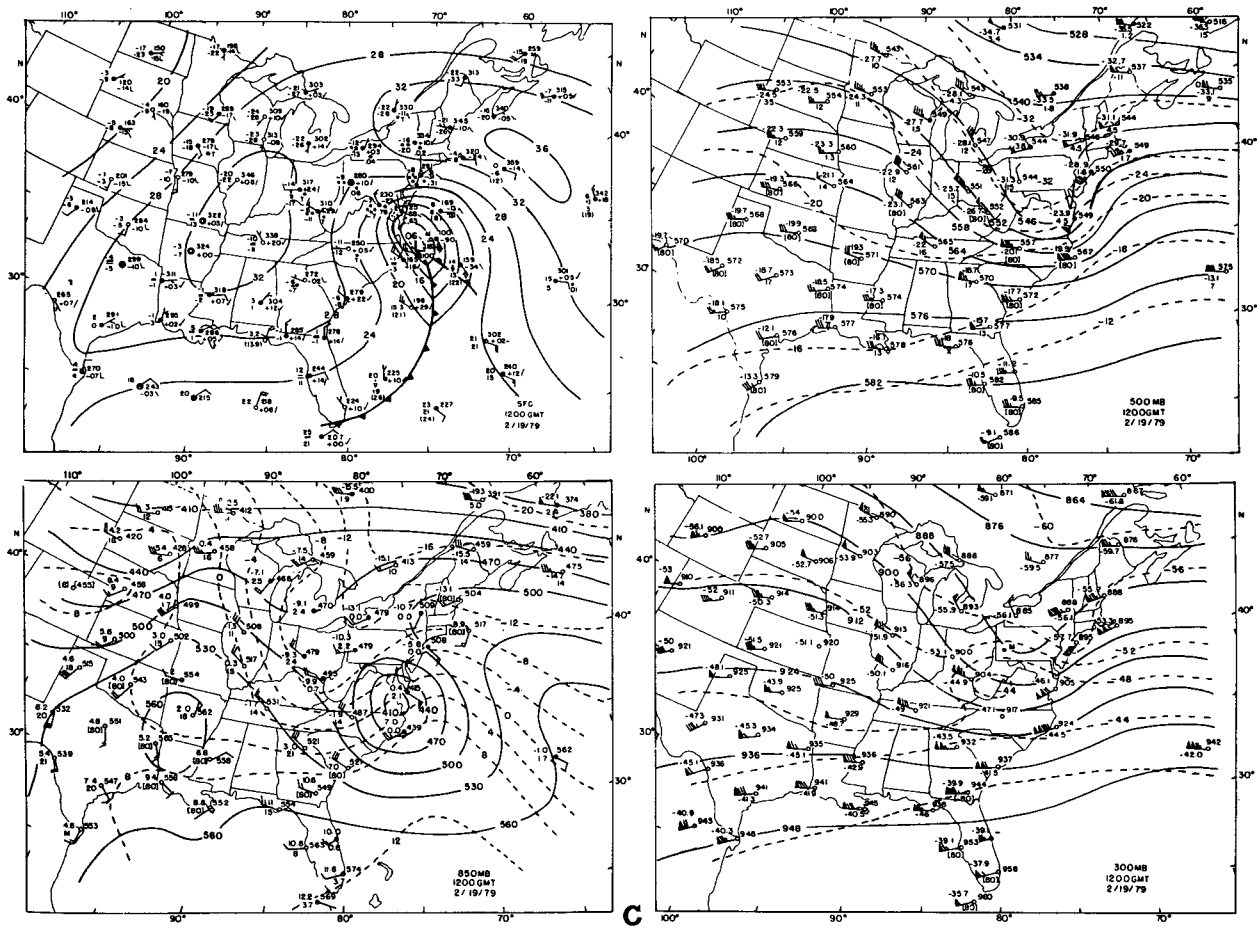


FIG. 1. (*Continued*)

yet to be seen in the vicinity of the Carolinas although a weak southern extension of the Ohio Valley trough, hinted at 12 h earlier, still is evident. At 300 mb a broad, strong west-southwesterly flow continues across the Atlantic seaboard with one isotach maximum center in the North Carolina-Virginia region and another center near Bermuda. This double center structure consolidates into one maximum east of Virginia at 250 mb (not shown).

In the following 12 h the offshore cyclone developed slowly north-northeastward, passing just to the west of Cape Hatteras. Strong surface intensification began just prior to 1200 GMT 19 February as the Ohio Valley short-wave trough reached the coast. Pronounced development and expansion of high, cold clouds reaching above 300 mb is noted in the infrared satellite pictures for the Ohio Valley trough during this period. A continued shortening of the half-wavelength of the 500 and 300 mb trough is seen.

A series of present weather and accumulated 6 h precipitation maps is shown in Fig. 2. Through 0000 GMT 19 February there is a slow eastward drift of the precipitation shield with the region of heaviest concentration moving east-northeastward between the Appalachians and the coast. After 0600 GMT the areal extent of the precipitation shield shrinks with heavy amounts confined to the Middle Atlantic States region, particularly centered around and just after 1200 GMT 19 February. During this latter period the locus of maximum precipitation parallels the western shore of Chesapeake Bay.

## 3. Quasi-geostrophic diagnosis

The track of the surface cyclone is illustrated in Fig. 3 (the moisture aspect of this figure will be discussed later). Rapid intensification occurred around 1200 GMT 19 February followed by storm curvature to the east. This is *opposite* to what is usually observed for deepening cyclones. Clearly the initial storm track is to the *left* of the instantaneous 500 mb flow (effective steering level is nearly the 850 mb surface) leading to a situation in which classical steering expectations would fail with un-

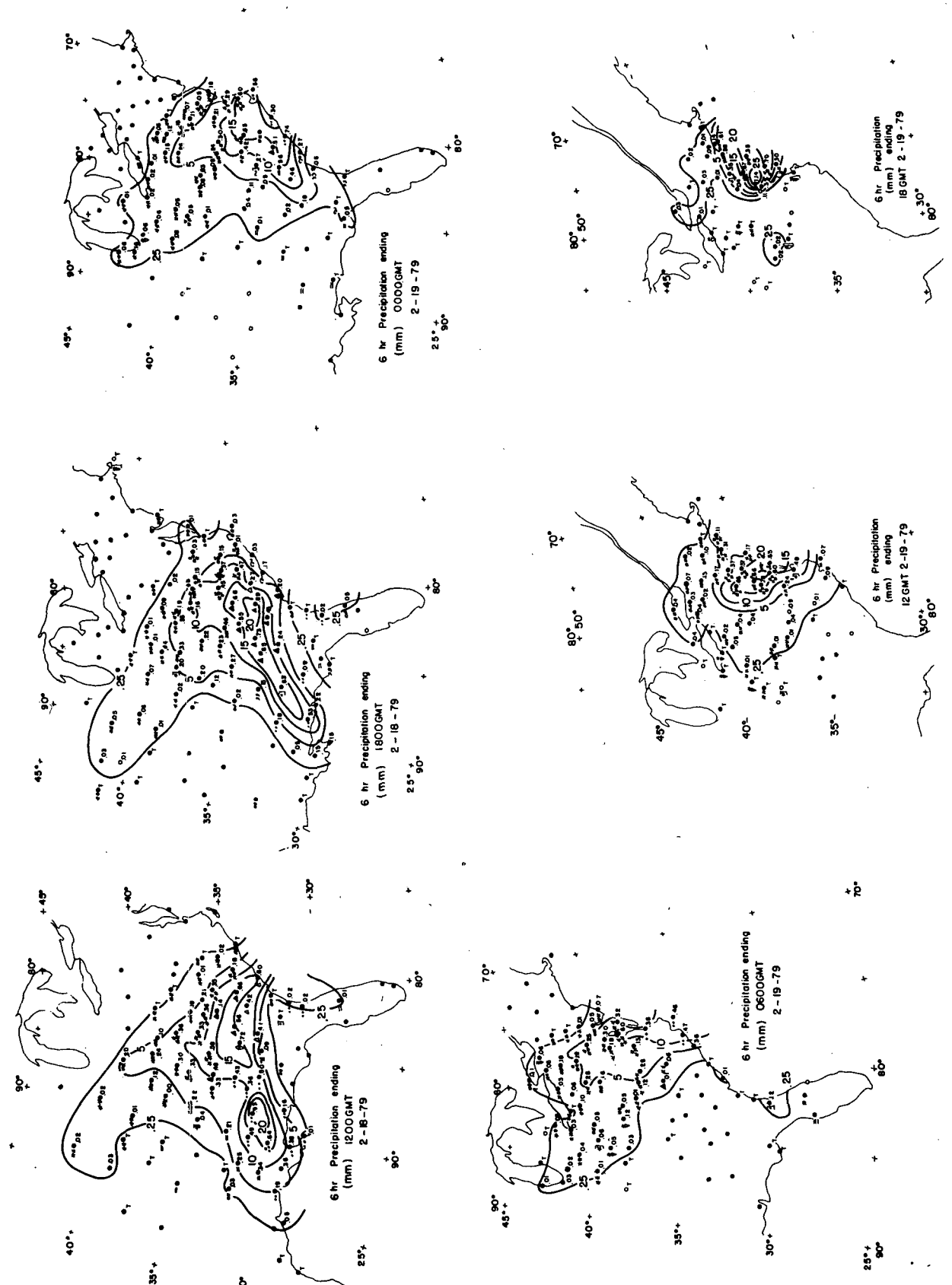


FIG. 2. Accumulated 6 h precipitation and present weather analysis for indicated times. Analyses in millimeters; raw observations for some stations plotted in hundredths of an inch (1 mm = 0.04 inch).

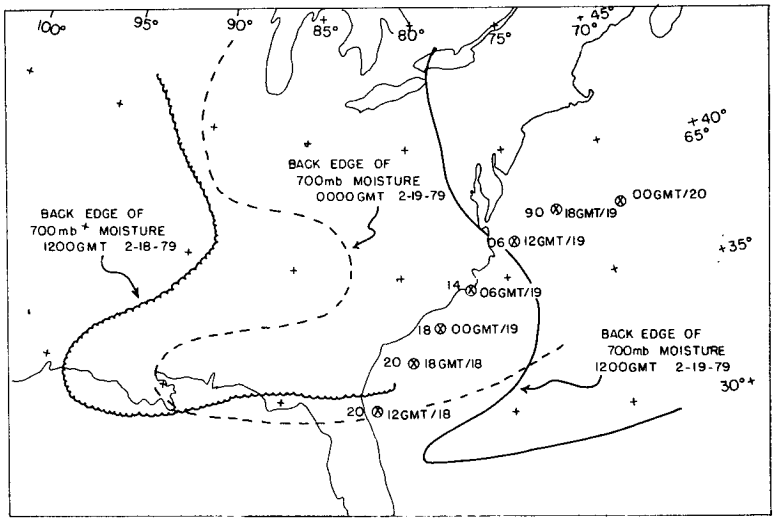


FIG. 3. Back edge of 700 mb high moisture area at indicated times and 6 h storm position indicated by a ⊗. Storm central pressure (mb) is given to the left of the ⊗ symbol.

fortunate forecast consequences. It appears that the cyclone initially did evolve along the coastal inverted trough. Then as the short wave moved east from the Ohio Valley the cyclone responded to larger scale forcing.

As an additional check on storm development, a 1000 mb quasi-geostrophic deepening rate applicable to the storm center was computed from the instantaneous conditions at 1200 GMT 19 February. The model employed was the Sanders and Gyakum (1980) version of the Sanders (1971) analytical model. The computation of the 1000 mb deepening rate from this model is given in Table 1. In the model the active deepening mechanism for middle-latitude cyclones is the positive thermal vorticity advection over the surface cyclone center. In Table 1 the term $a$ is a measure of the basic planetary-scale north–south temperature gradient while $T$ represents the perturbed part of this temperature field. Additional parameters include $n_0$ (the domain-averaged absolute vorticity), $f_0$ (the map-averaged Coriolis parameter), $T_0$ (the mean tropospheric temperature), and $L$ (the wavelength of the synoptic-scale thermal perturbation defined by the 1000–500 mb thickness field). Here $\gamma$ is a dimensionless static stability parameter while $\lambda$ measures the distance from the downstream thermal ridge to the upstream cyclone center. See Sanders and Gyakum (1980) for more specific information on computational procedures.

The $\gamma$ values of 0.190 and 0.016 were derived by referring the 1200 GMT 19 February Cape Hatteras sounding (850–500 mb layer) to a dry and moist adiabat, respectively. This sounding is most representative of the storm core environment at that time. The value of $\gamma = 0.063$ corresponds to a 72-sounding average for rapidly deepening oceanic cyclones obtained by Sanders and Gyakum (1980).

The computed deepening rate most closely matches the observed deepening rate when the observed temperature profile at Cape Hatteras is referenced to the moist adiabat. Sounding data support a moist structure to just above 700 mb with very dry conditions above that level. Satellite infrared pictures do not support the presence of a deep, saturated layer in the storm center environment.

However, the agreement between theory and observation has probably been overstated because the requirement of a saturated atmosphere and the neglect of frictional mass inflow has yielded the maximum possible deepening from the quasi-geostrophic model. As a further check on these computations, Tracton (private communication) has employed a 10-level quasi-geostrophic model on the

TABLE 1. Computed versus observed surface cyclone 6 h instantaneous deepening rate [mb (6 h)$^{-1}$] after Sanders and Gyakum (1980).

| | |
|---|---|
| $L$ | 1444 km |
| $a$ | $1.44 \times 10^{-5}$ K m$^{-1}$ |
| $\hat{T}$ | 6.4 K |
| $f_0$ | $0.88 \times 10^{-4}$ s$^{-1}$ (37.5°N) |
| $\eta_0$ | $1.03 \times 10^{-4}$ s$^{-1}$ |
| $T_0$ | 250 K |
| $\lambda/L$ | 0.10 |
| Observed deepening rate | 16.0 mb (6 h)$^{-1}$ |
| Calculated deepening rate (dry) | 1.9 mb (6 h)$^{-1}$, $\gamma = 0.190$ |
| Calculated deepening rate (moist) | 13.6 mb (6 h)$^{-1}$, $\gamma = 0.016$ |
| Calculated deepening rate (oceanic cyclogenesis climatology) | 5.5 mb (6 h)$^{-1}$, $\gamma = 0.063$ |

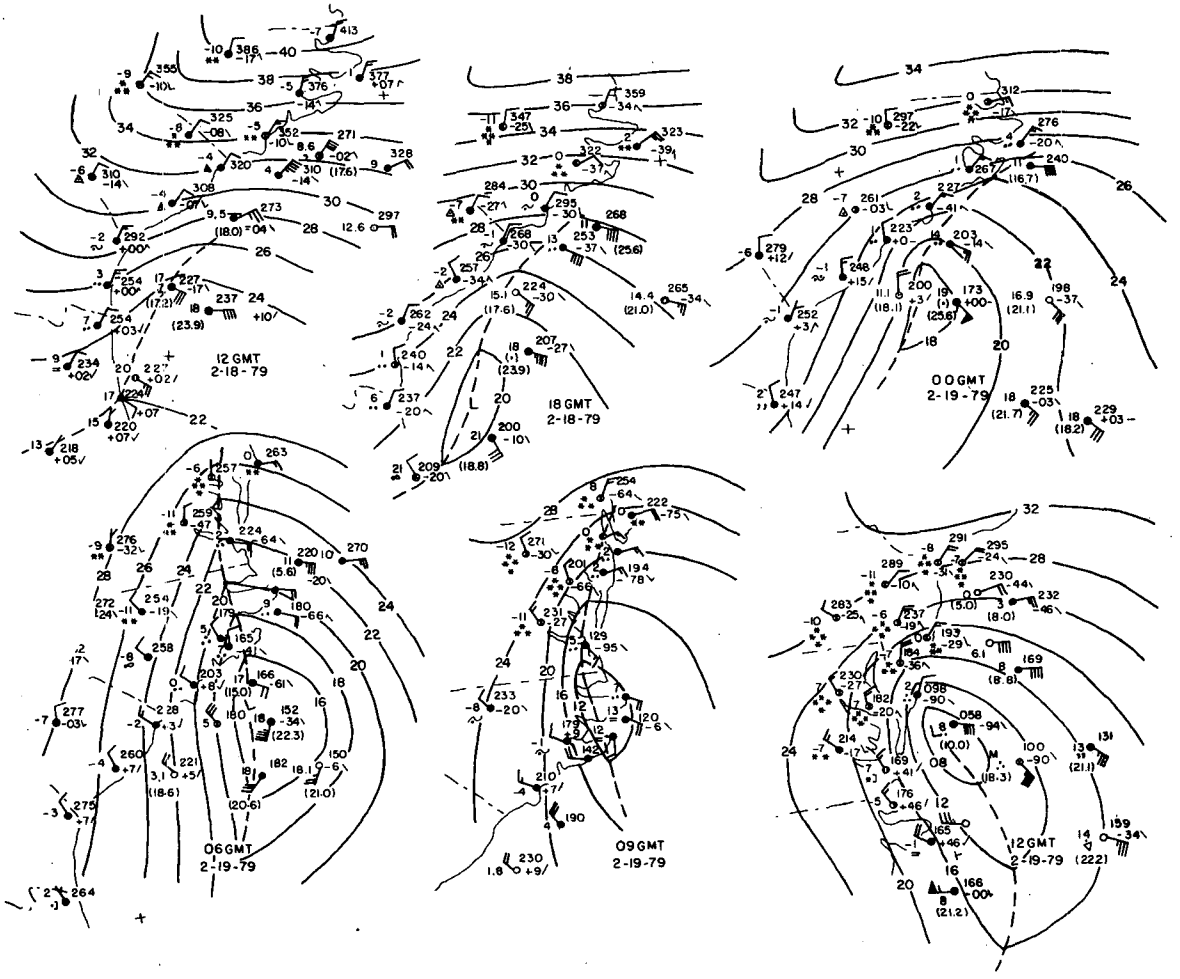


FIG. 4. Surface sectional plots illustrating coastal front structure for 1200 and 1800 GMT 18 February and 0000, 0600, 0900 and 1200 GMT 19 February 1979. Winds in m $s^{-1}$ (Fig. 1 convention) and temperatures in °C. Surface isobars (mb) are given by solid lines; coastal front position illustrated by dashed lines. Open circles over ocean indicate buoys for which no present weather is available. Ocean temperatures (°C) are given in parentheses.

operational LFM analyses for this same time period. He computes an instantaneous deepening of 6.6–7.8 mb (6 h)$^{-1}$ with the difference attributable to the location of the cyclone with respect to the grid mesh in the initial analysis. Stable heating accounts for 10–15% of the computed deepening rate. Frictional filling is ignored. Evidently, there are other important physical factors beyond the scope of the quasi-geostrophic model that are relevant to explaining the rapid cyclogenesis. Quasi-geostrophic forcing, however, is certainly in the right direction and of qualitative use in understanding the cyclonic development.

Moreover, the operational NMC LFM-II and 7LPE models also failed to capture the cyclogenesis despite presumably superior physics. Sanders and Gyakum (1980) found similar results for many cases of oceanic cyclogenesis. This suggests that oceanic cyclogenesis probably responds to a combination of subtle physical factors either absent or improperly treated in existing operational primitive equation models. Initial analysis inadequacies bring about additional uncertainty. Tracton (1973) has suggested that failure to treat the bulk effects of convection near the incipient storm center prevents the operational models from properly simulating explosive oceanic cyclogenesis. Some evidence for this possibility in the present case is given in Section 7.

## 4. Mesoscale description of the coastal front

Fig. 4 affords a detailed mesoscale sectional view of the developing coastal cyclone. Broad onshore flow is seen at 1200 GMT 18 February with a well defined wind shift extending from just north of Daytona Beach, Florida to the area east of the Georgia coast. The ship data are rather persuasive in this respect with the temperature contrast averaging

10°C (100 km)$^{-1}$ across the incipient front. In the following 6 h the coastal front continues to increase in intensity with a strong convergence zone extending well northward to off of the North Carolina coast. By 0000 GMT 19 February a closed cyclonic circulation is evident with continued strong thermal contrast in the coastal zone. The developing cyclone center is approaching the North Carolina coast at 0600 GMT with the coastal front now extending northward just west of Norfolk, Virginia to the lower Chesapeake Bay. From 0900 to 1200 GMT the cyclone center passes west of Cape Hatteras and on into the western Atlantic as explosive deepening occurs. The coastal front reaches up into the northern Chesapeake Bay area at 0900 GMT and then retreats seaward after 1200 GMT in response to strong offshore cyclogenesis.

Figs. 5–7 depict hourly time sections at selected locations to further illustrate the strength and importance of the coastal front on the mesoscale weather patterns. Through 1200 GMT 18 February a broad northeasterly flow embedded in a zone of strong temperature contrast is seen at Charleston, South Carolina and the westernmost ocean buoy about 100 km offshore (Fig. 5). The wind veers abruptly between 1200 and 1300 GMT and the temperature increases accordingly at the buoy as the coastal front becomes established. Further veering

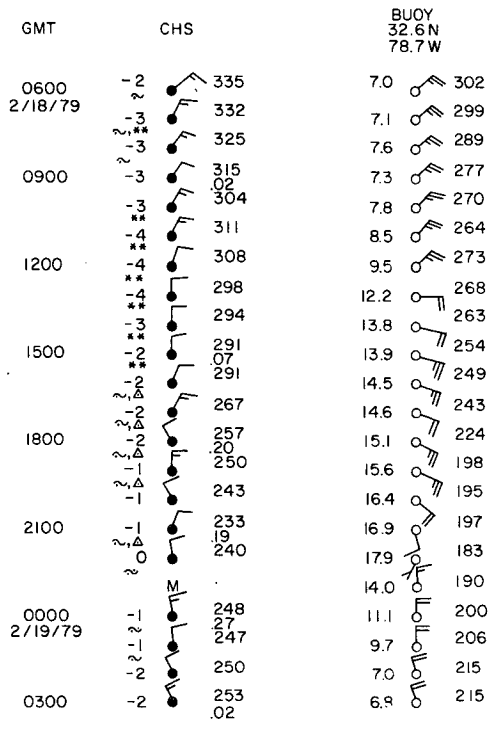


FIG. 5. Time section of temperature (°C), pressure (mb) and winds (m s$^{-1}$, Fig. 1 convention) for Charleston, South Carolina (CHS) and an ocean buoy located at 32.6°N, 78.7°W.

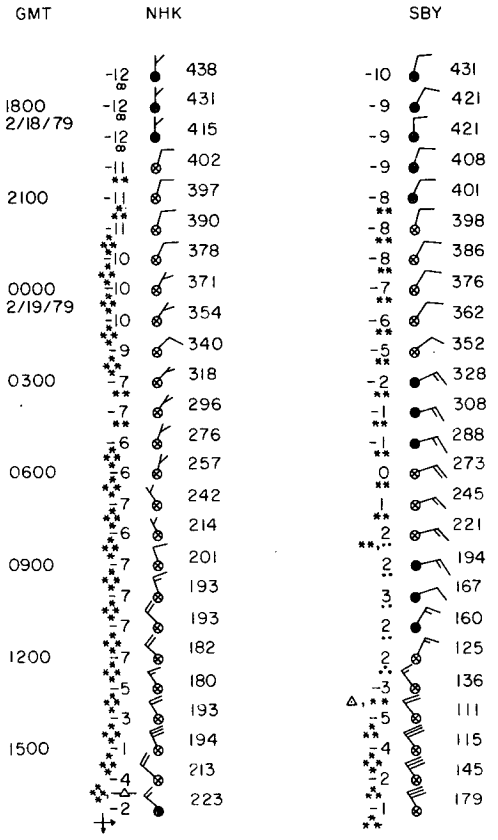


FIG. 6. As in Fig. 5 except for Patuxent River, Maryland (NHK) and Salisbury, Maryland (SBY).

takes place in the ensuing hours until finally the developing cyclone passes just to the west of the buoy at 2200 GMT. Meanwhile the winds at Charleston exhibit a slight backing tendency as directional convergence increases into the coastal front zone prior to the arrival of the surface cyclone.

Fig. 6 shows the situation at two stations on opposite sides of Chesapeake Bay. The coastal front circulation is first evident around 0300 GMT as winds veer to the east and back to the west on opposite sides of the Bay. Note the changeover to rain at Salisbury where precipitation remains light while Patuxent River to the west is overwhelmed with 12 h of continuous heavy snow. Heavy precipitation is not seen at Salisbury until the coastal front retreats seaward after 1200 GMT and winds back around to northwesterly. This relationship between the wind and precipitation field is remarkably similar to New England coastal front studies by Bosart *et al.* (1972), Bosart (1975) and Marks and Austin (1979). Similar results are also seen farther north. Both Dover, Delaware and Atlantic City, New Jersey (Fig. 7) do not report their heaviest sustained precipitation until the coastal front passes these lo-

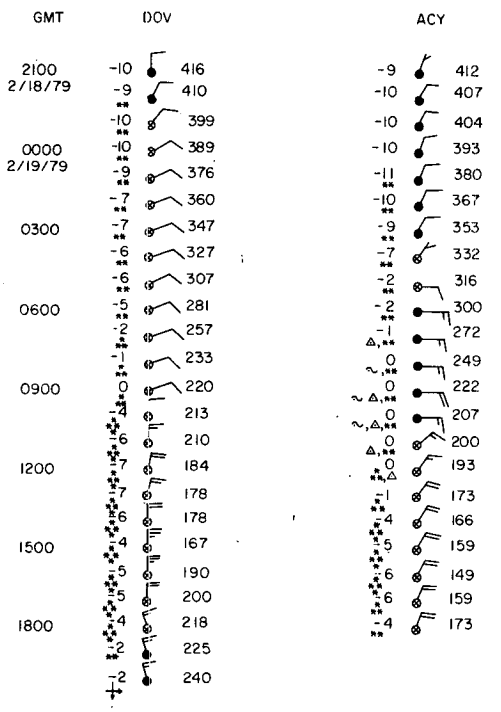


FIG. 7. As in Fig. 5 except for Dover, Delaware (DOV) and Atlantic City, New Jersey (ACY).

cations while retreating seaward. Strongly ageostrophic surface winds with cross-contour flow angles averaging 50–60° in the cold air help to force the front eastward against the persistent easterly flow north of the developing cyclone center.

### 5. Radar observations of the coastal front

Radar observations were next examined to extract more information about mesoscale details of the precipitation field. National Weather Service (NWS) WSR-57 radar film records and logs were obtained for Daytona Beach, Florida, Charleston, South Carolina, Wilmington and Cape Hatteras, North Carolina, Patuxent River, Maryland and Atlantic City, New Jersey. The well-defined wind shift line east of Georgia and Florida at 1200 GMT 18 February corresponds to a broken line of echoes with tops to 625 mb as seen from Daytona Beach radar (not shown). Individual cells are moving from 130° at 6 m $s^{-1}$. Echo intensities are computed as between 3 and 12 mm $h^{-1}$. This broken line of showers becomes organized into a nearly solid line of showers with some embedded thunderstorms (echo intensities up to 25 mm $h^{-1}$) between 1700 and 2000 GMT before gradually weakening and moving eastward out of radar operational range. Meanwhile, new prefrontal convective activity developed over the ocean shortly before 0000 GMT 19 February and continued for the next 9 h.

Charleston radar detects on and off slight showers of snow, ice pellets and rain eastward over the ocean from the 17th onward in the cold onshore air stream. Between 0000 and 0600 GMT 18 February a general area of light precipitation (echo intensities $< 2.5$ mm $h^{-1}$) including snow, ice pellets and freezing rain is seen by Charleston radar from the coastal zone westward. This area persists and slowly intensifies over the next 12 h with some echo intensities reaching 12.5 mm $h^{-1}$. Simultaneously, a band of echoes 20–30 km wide is detected 80–100 km offshore and parallel to the coast. This coastal front precipitation band tends to move slowly northwestward while partially merging with the main precipitation shield. Throughout the Charleston radar history of the storm, however, the echoes maintain a well-defined oceanic edge in approximately the position of the surface coastal front. Similar behavior is observed by the Wilmington radar.

Cape Hatteras radar detects the offshore coastal front precipitation band shortly before 1200 GMT 18 February. The echo characteristics are similar to that seen farther south. Some of these echoes reach an intensity level of 25 mm $h^{-1}$ between 0000 and 0600 GMT 19 February as the offshore line moves landward to merge with the onshore precipitation pattern. This line disappears entirely after 0700 as surface winds at Cape Hatteras veer to southeasterly in the warm sector of the developing cyclone. A major development is radar detection of a new north–south oriented line of echoes 25 km wide and 70 km long centered 60 km to the west-southwest of the radar between 0700 and 0800 GMT. This line intensifies slowly and expands northward and southward before crossing the radar location just before 1100 GMT. Vigorous thunderstorms developed along this line, representing the main cold front, between 1200 and 1300 GMT just east of Cape Hatteras. More will be said about this development in the next section.

Patuxent River radar reveals a nearly stationary line of enhanced echoes centered over Chesapeake Bay coincident with the time of reported heavy snow at Patuxent River (NHK in Fig. 6). The activity is strongest from Patuxent River northward. To the south the echo pattern is more irregular except for a period around 1200 GMT 19 February when an increasingly well-defined line containing moderate rain showers is detected moving eastward. This line probably represents a northward extension of the previously discussed Cape Hatteras line.

Finally, Atlantic City radar detects a rather vigorous band of convection south and east of the radar site between 1000 and 1430 GMT (time of radar failure). Echo intensities reach 50–100 mm $h^{-1}$ in this band. The westward extension of this area is reported as a very heavy snow band which reached

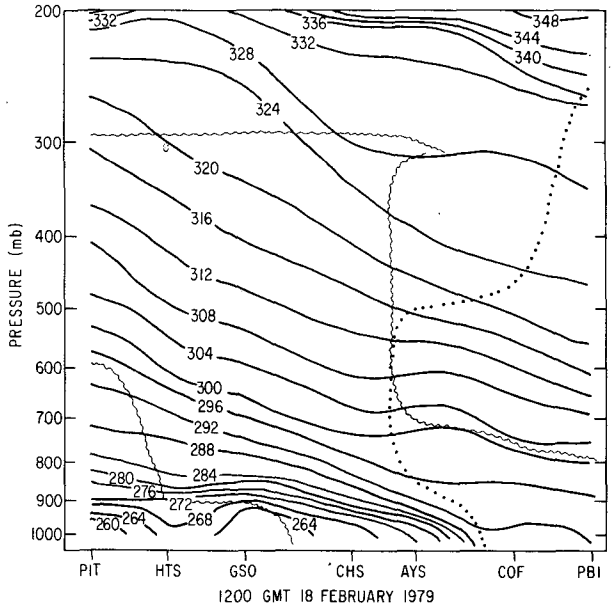


FIG. 8. Cross section of potential temperature °K, solid lines along 80°W from Pittsburgh, Pennsylvania (PIT) to West Palm Beach, Florida (PBI) for 1200 GMT 18 February 1979. Escalloped lines enclose regions of relative humidity ≥ 70%. Convectively unstable region is enclosed by the dotted line.

to the Dover, Delaware vicinity. It seems to coincide with the wind shift line separating easterly from northerly flow.

In summary, the radar data supports the coastal front as a persistent entity embedded in a general precipitation area which expands northward and westward in response to the approach of the Ohio Valley short-wave trough.

## 6. Coastal front structure

Fig. 8 is a cross section of potential temperature and moisture along 80°W at the time of incipient coastal frontogenesis. A general south-to-north temperature decrease overlies an extremely cold and stable boundary layer. The coastal front appears as a well-defined feature which is generally confined below 850–900 mb. Note the apparent damming effect of the Appalachians with cold air especially entrenched near Greensboro, North Carolina (GSO).

A detailed cross section of wind and potential temperature (surface to 700 mb) between Athens, Georgia (AHN) and Cape Canaveral, Florida (COF) for 1200 GMT 18 February is shown in Fig. 9. The orientation of the line is from 330 to 150° which is nearly normal to the lower tropospheric isotherms which closely parallel the front. Wind components are resolved into this plane using horizontal analyses in order to perform kinematic vertical motion, frontogenesis and vorticity tendency equation computations. The assumption is made that across-front

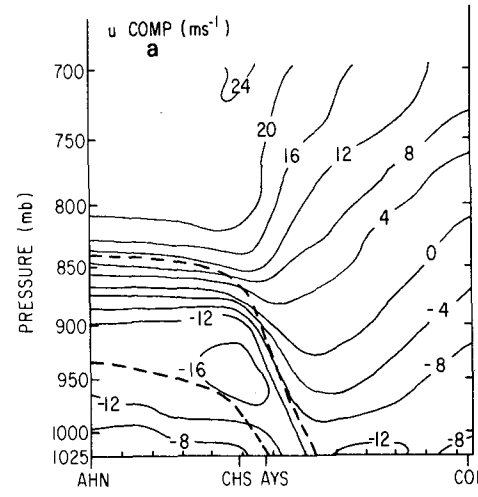


FIG. 9a. Surface to 700 mb cross section of wind speed (m s$^{-1}$, solid lines) normal to the section for 1200 GMT 18 February. The section is oriented along an approximate line 330–150°. Dashed lines denote upper ($\theta$ = 290 K) and lower ($\theta$ = 270 K) boundaries of coastal front zone.

variations are much greater than along-front variations in all computations. A horizontal and vertical mesh length of 25 km and 25 mb is employed for all data reduction.

The following quantities are evaluated using centered differences:

$$\frac{\partial \omega}{\partial p} = -\frac{\partial v}{\partial y}, \tag{1}$$

$$\frac{d}{dt}\left(-\frac{\partial \theta}{\partial y}\right) = +\frac{\partial v}{\partial y}\frac{\partial \theta}{\partial y} + \frac{\partial \omega}{\partial p}\frac{\partial \theta}{\partial y} - \frac{\partial}{\partial y}\left(\frac{d\theta}{dt}\right), \tag{2}$$

$$\frac{d}{dt}\left(-\frac{\partial u}{\partial y}\right) = \frac{\partial v}{\partial y}\frac{\partial u}{\partial y} + \frac{\partial \omega}{\partial y}\frac{\partial u}{\partial p} - f\frac{\partial v}{\partial y} - \frac{df}{dt}, \tag{3}$$

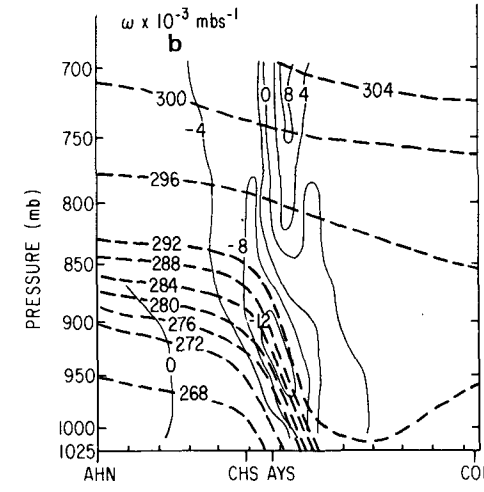


FIG. 9b. As in Fig. 9a except for vertical motion ($\times 10^{-3}$ mb s$^{-1}$, heavy solid lines) superimposed on the potential temperature field (K, thin solid lines).

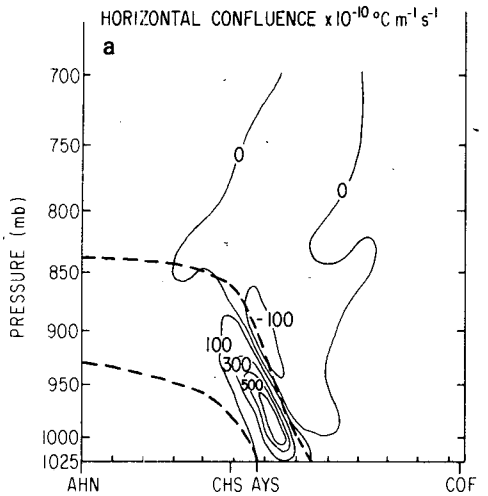


FIG. 10a. As in Fig. 9a except for contribution of horizontal confluence ($\times 10^{-10}$ °C m$^{-1}$ s$^{-1}$, thin solid lines) to frontogenesis. Multiply by $10^8$ to convert units approximately to °C (10 km) (3 h)$^{-1}$.

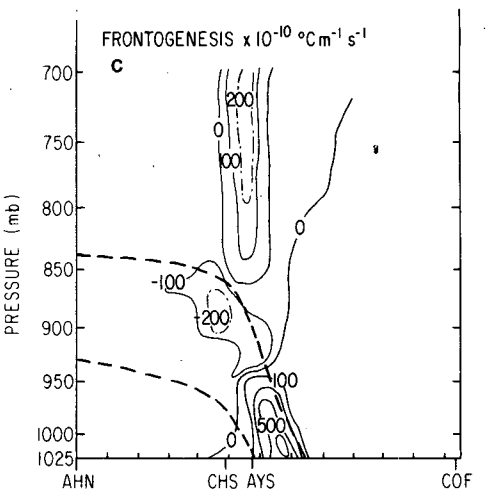


FIG. 10c. As in Fig. 10a except for the total frontogenesis field.

where all the symbols have their usual meteorological meaning. In all computations the $y$ axis is taken positive toward colder air while $\omega$ is taken as zero along the bottom boundary. The diabatic term in (2) and the beta-effect term in (3) are not evaluated.

The wind component perpendicular to the cross section is shown in Fig. 9a while the result of the kinematic omega computation is shown in Fig. 9b. In both cases, dashed lines representing the $\theta = 290$ and 270 K surfaces delineate the coastal front zone. Strong lateral wind shear along the warm boundary of the frontal zone near 950 mb is indicated while considerable vertical wind shear is found above the front. Strong ascent in excess of $-12 \times 10^{-3}$ mb s$^{-1}$ centered near 950 mb toward the warm boundary of the coastal front is shown. A narrow tongue of ascent is found well above the frontal surface. Overall the vertical motion picture is remarkably similar to that found by Sanders (1955) for an intense surface frontal zone. The wind components in the plane of the diagram show flow in the cold air toward the front while in the warm air to the east and aloft, the flow is onshore. This yields a simple, thermally direct mesoscale circulation as defined by a mass streamfunction (not shown) in the $yp$ plane similar to the classic thermally direct circulations of Sawyer (1956) and Eliassen (1962) for larger scale frontal regions.

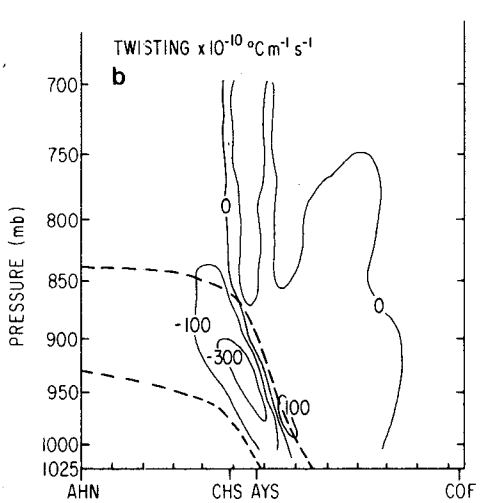


FIG. 10b. As in Fig. 10a except for the twisting term.

This finding certainly suggests precipitation enhancement on the cold side of the surface frontal zone which is suggested by radar and conventional data in the present case, and has been deduced by Bosart (1975) and Marks and Austin (1979) for other cases. Ballentine (1980) has produced the same effect in a numerical investigation of coastal frontogenesis. Microphysical processes working in tandem with the frontal dynamics may be an additional source of precipitation enhancement. A hypothesis of some type of seeder-feeder process as originally envisioned by Bergeron (1949) and refined most recently by Hobbs *et al.* (1980) and Herzegh and Hobbs (1980) is attractive on physical grounds. Confirmation must await more detailed radar and aircraft investigations of active coastal fronts.

Frontogenesis computations according to (2) are depicted in Fig. 10a–10c. Horizontal confluence (Fig. 10a) is strongly frontogenetical within the frontal zone. The maximum contribution is located just above the surface and then decreases upward. Peak values approach 9°C (10 km)$^{-1}$ (3 h)$^{-1}$. The twisting term (Fig. 10b), on the other hand, is strongly frontolytical within the frontal zone except on the immediate warm boundary of the zone and

in a narrow region above the front. The total frontogenesis function exclusive of diabatic effects (Fig. 10c) shows a strongly frontogenetical region below 950 mb yielding to a frontolytical area above this level. This suggests a rapid decrease in coastal front intensity upward consistent with Sanders' (1955) findings for an intense surface front.

To the extent that the overall pattern can be viewed as quasi-stationary (supported by the surface and radar observations), it appears that air parcels approaching the coastal front from the east are forced to ascend while remaining essentially in the warm air. Meanwhile, air parcels on the cold side of the frontal zone gradually acquire the thermal and moisture characteristics of the underlying sea surface as they move farther offshore. These latter air parcels then begin to ascend and return toward the coast as the entire frontal zone slowly shifts coastward. The strongly ageostrophic cross-frontal circulation acts to provide a continuously renewable supply of cold air whose source is produced by damming to the east of the Appalachian Mountains. This acts to oppose the westward drift of the frontal zone implied by the low-level geostrophic flow (recall Fig. 4). The picture is consistent with that found by Ballentine (1980) in a numerical investigation of New England coastal frontogenesis as well as the observational studies of Baker (1970) and Richwien (1980).[3]

The coastal front is different from the intense surface front discussed by Sanders (1955) in that while in the cold air there is a wind component toward the front, the front does not move progressively toward warmer air. In this sense, the coastal front acts like a warm front which progressively moves toward colder air despite normal wind components in the cold air toward the front. When this happens with a warm front over land, the available evidence suggests that warmer air from aloft mixes down to the surface in a series of gusts or pulses. Spar (1956) showed this was the case in a detailed mesoanalysis of a warm front passage along the east coast. On several occasions the author has witnessed abrupt southerly surges in association with warm frontal passages 5–10 min after low scud 100–200 m above the ground is discernible streaming out of the south at speeds of 15–25 m $s^{-1}$. While it is possible that such turbulent mixing is operating in the coastal front situation, it seems more likely that the cold, stable boundary-layer air over the land is slowly destabilized as it moves over the ocean by sensible and latent heat fluxes with continued erosion of the seaward edge of the stable portion of the boundary layer. Without the cold-air mound banked up against the Appalachians, the coastal front would undoubtedly be both weaker and far more able to penetrate inland with the easterly geostrophic current.

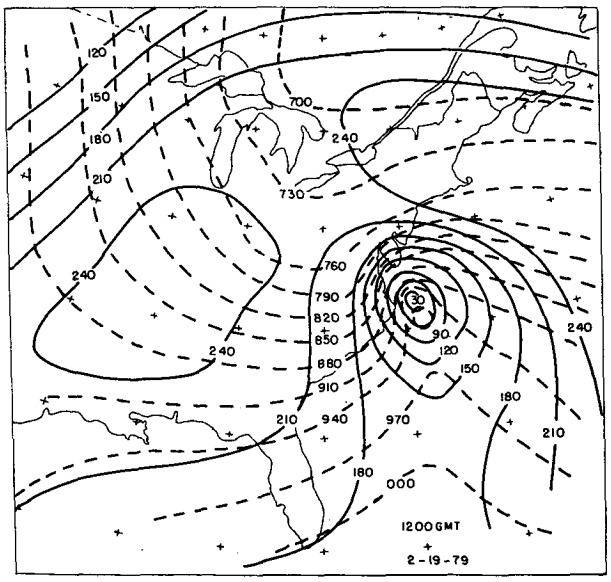


FIG. 11. 1000–700 mb thickness (dam, dashed lines) and 1000 mb heights (m, solid lines) for 1200 GMT 19 February 1979.

The vorticity structure according to (3) (not shown) establishes that the horizontal shear or confluence term is analogous to the corresponding effect in (2) and contributes to vorticity generation within the frontal zone. Meanwhile the vertical shear contribution which is analogous to the twisting effect in (2) contributes to vorticity destruction within the frontal zone except along the warm boundary and near the cold boundary just above the surface. The Coriolis effect is somewhat smaller but still contributes to vorticity growth within the frontal region. The total vorticity tendency reveal growth (destruction) within the frontal zone below (above) 925 mb with a separate area of generation in the warm air above the zone. Evidently, the growth of vorticity and temperature contrast within the frontal zone is concentrated in the very lowest layers of the atmosphere. The appearance of a frontal zone at higher levels (e.g., 850 mb) must be associated with a vertical circulation which transports air parcels upward that have acquired frontal characteristics near the surface.

## 7. Evidence for convective influences in cyclogenesis

During the period 1200–1800 GMT 19 February the cyclone underwent an explosive deepening of ~16 mb while acquiring a vortex structure through a relatively deep tropospheric layer. Fig. 11 suggests that at the outset of major deepening, the cyclone environment was nearly warm core as determined from a subjective 1000–700 mb thickness

[3] Richwien, B. A., 1980: The damming effect of the southern Appalachians. *Nat. Wea. Dig.*, 5, 2–12.

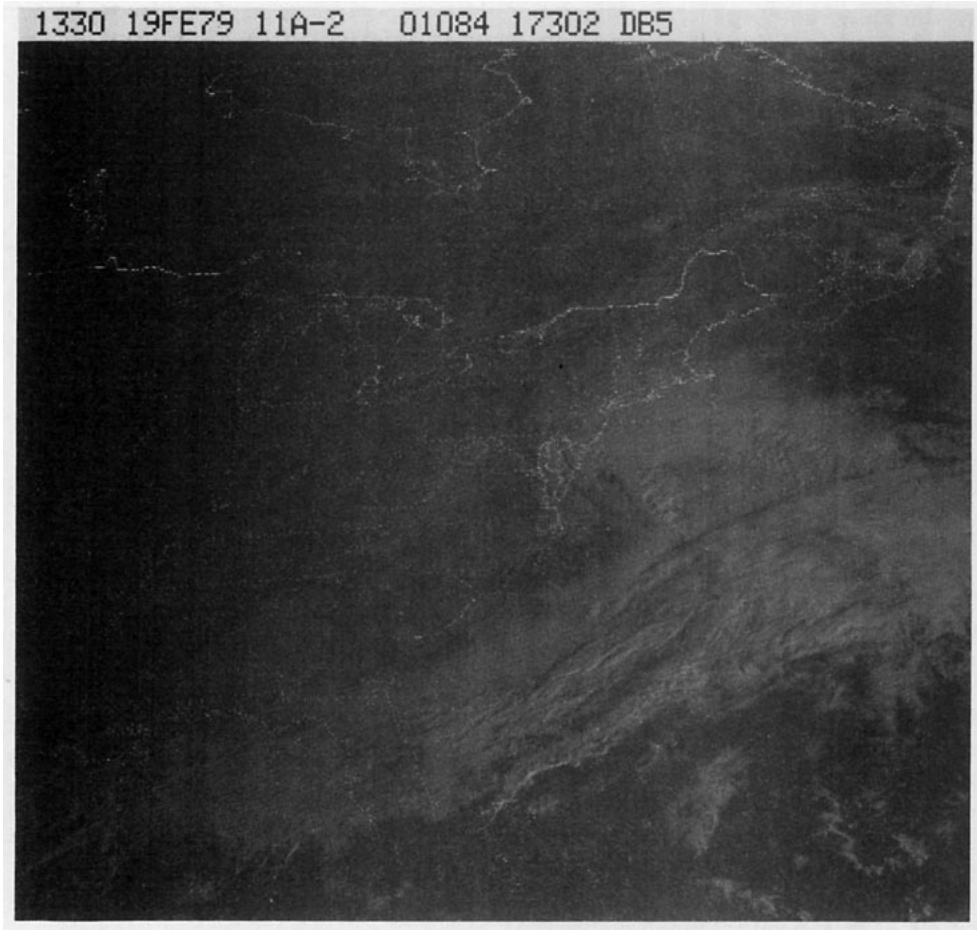


FIG. 12. Visible GOES satellite picture valid 1330 GMT 19 February 1979. (Misgridding: Shift geography eastward ~125 km relative to picture.)

analysis, a situation not unlike that of a tropical storm. The available evidence hints strongly that convective processes probably play an important role in the rapid intensification. A solid line of thunderstorms with tops extending to 300 mb is observed by Cape Hatteras radar at 1235 GMT 19 February along a NNW–SSE line just to the east of the station. This line develops rather suddenly during the previous hour from a band of precold frontal echoes that originally form around 0700 GMT. Coincident with the onset of convection was the arrival of dry air at 700 mb just to the west of the surface cyclone position as represented by the back edge of a middle cloud layer. Clear evidence is seen in the 1330 GMT visible satellite picture (Fig. 12) for this NNW–SSE oriented line of active convective cells.

Fig. 13 shows the profile of equivalent potential temperature ($\theta_e$) at Cape Hatteras as determined from the regular 1200 GMT 19 February sounding (actual launch 1110 GMT). A layer of convective instability between 850 and 500 mb overlays a very stable boundary layer. The profile is somewhat misleading, however, in that Cape Hatteras reported a cold frontal passage accompanied by heavy rainshowers, a temperature decrease from 15 to 3°C, and a wind shift from southeast to west-northwest 25 min before the radiosonde launch. The solid line is an estimated $\theta_e$ profile in the warm storm center environment just ahead of the developing convective line. It is based on an assumed moist adiabatic lapse rate under saturated conditions from the given surface temperature. This atmosphere is clearly capable of supporting convection given an appropriate lifting mechanism.

More direct evidence is offered in Fig. 14 which shows kinematic omega profiles for the Wallops Island–Cape Hatteras–Greensboro triangle valid at 1200 GMT 19 February. The profiles are computed from wind data available at the surface, 1000 mb and every 50 mb thereafter to 100 mb. The vertical motion is assumed to vanish at the lower boundary. A constant correction is applied to the divergence based upon the method of O'Brien (1970) to ensure zero vertical motion at 100 mb. The dashed line represents the omega profile from the regular data

while the solid line corresponds to a modified profile assumed valid at Cape Hatteras prior to the surface wind shift at 1045 GMT. The Cape Hatteras surface to 850 mb wind profile is reconstructed based on the reported prefrontal surface wind and the low-level winds at Wallops Island. In either profile, the result suggests a low-level (800 mb) ascent maximum capped by subsidence in the mid and upper troposphere. The modified omega profile clearly is capable of supporting the growth of convective elements in the storm environment.

Figs. 15–17 (Unavoidable operational problems resulted in misgridding of these pictures—Fig. 16 is off while Figs. 15 and 17 are misgridded in opposite directions. Use the Great Lakes and Florida for eyeballing geographical corrections) show visible satellite pictures at 1530, 1830 and 2130 GMT which demonstrate the presence of convective processes accompanying rapid deepening and vortex generation. Fig. 16 is especially dramatic in that it shows a well-defined "eye-like" structure reminiscent of a tropical cyclone. This phenomenon has been observed in other winter ocean cyclones, most recently on 7 February 1978 and 3 March 1980 in connection with New England and North Carolina blizzards. The development of the eye is suggested 3 h earlier and it is also detected in the IR pictures (not shown). The sunset picture at 2130 GMT nicely

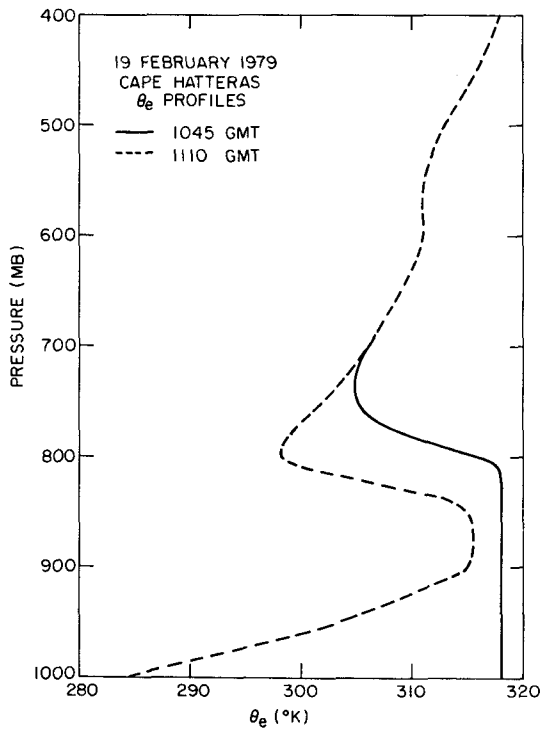


FIG. 13. Equivalent potential temperature profiles ($\theta_e$, K) at Cape Hatteras, North Carolina valid 1045 and 1110 GMT 19 February 1979. See text for further explanation.

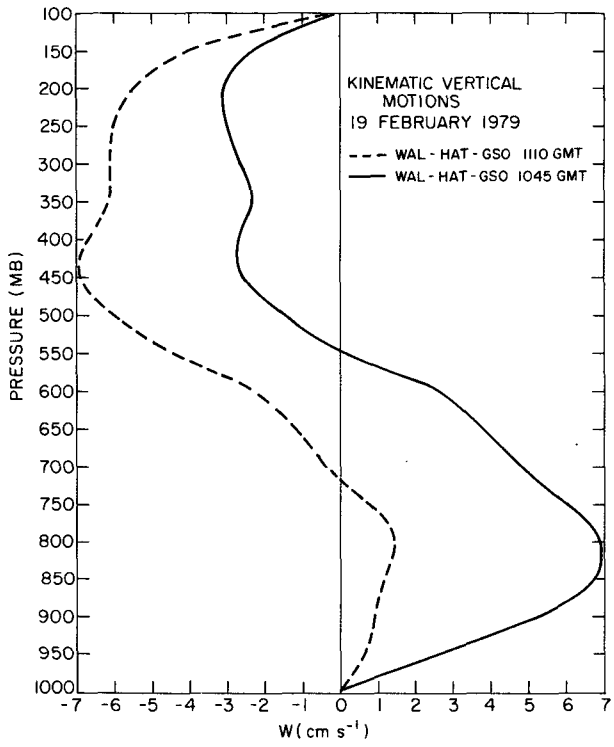


FIG. 14. Kinematic omega profile (expressed in cm s$^{-1}$) for the centroid of the triangle defined by Wallops Island, Virginia (WAL); Cape Hatteras, North Carolina (HAT), and Greensboro, North Carolina (GSO) for the indicated times. See text for further explanation.

illustrates the well-defined convective bands feeding into the northern half of the storm.

Developments at the surface during this time period are equally dramatic. Fig. 18 is a detailed composite surface map for the 1700–1800 GMT period 19 February based on Baltimore Canyon drilling rig data, marine data from NMC and ships logs from the National Climatic Center (NCC). Weather conditions are somewhat less than ideal for ocean cruising. Sustained winds are exceeding hurricane force at several locations with reported wave heights in excess of 12 m. The pressure gradient is especially tight to the west of the storm center and approaches 1 mb (5 km)$^{-1}$. Additional deepening probably occurs in the ensuing 6 h but sparse ship coverage in the storm vicinity precludes a definitive statement.

The accumulated evidence suggests that convection plays a significant role in the explosive development phase of the cyclone commencing around 1200 GMT 19 February. Quasi-geostrophic forcing from the approaching Ohio Valley trough is instrumental in initiating cyclogenesis through a deep tropospheric layer but appears incapable of accounting for the rapid transformation of the cyclone to a vortex structure in 6 h, consistent with the expected underdevelopment noted earlier. A climatology of

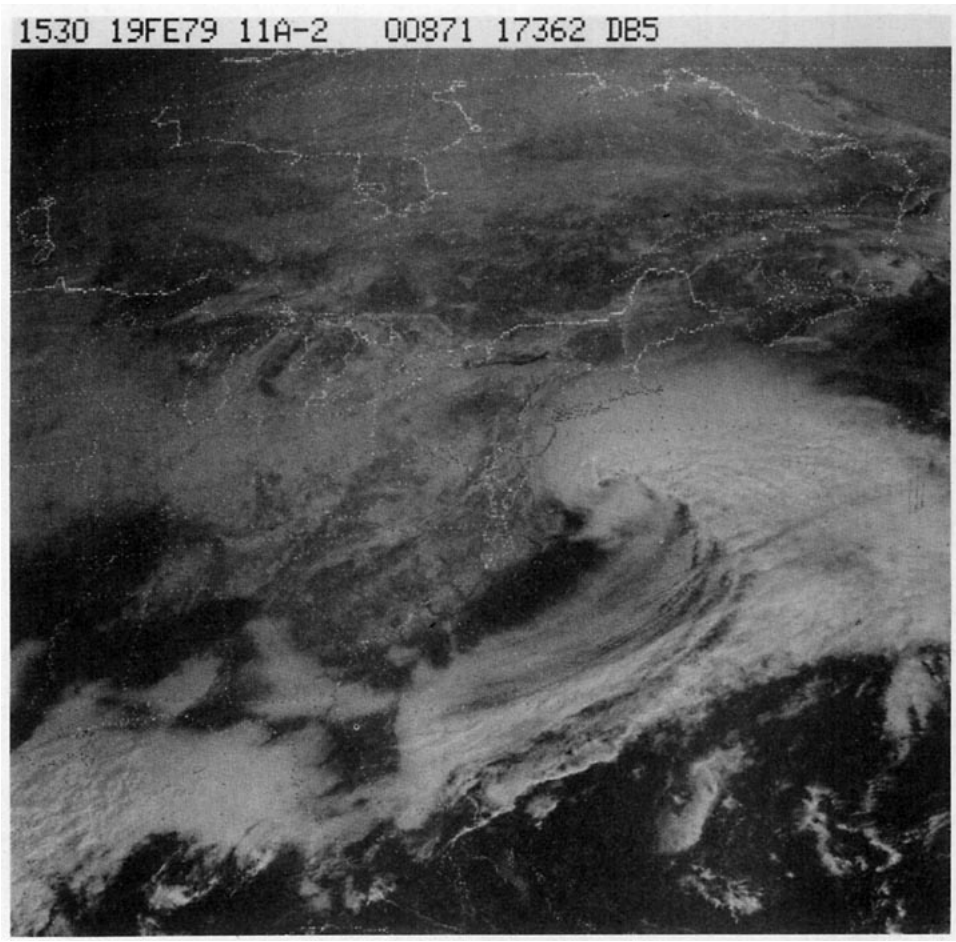


FIG. 15. As in Fig. 12 except for 1530 GMT 19 February 1979. (Misgridding: Shift geography eastward ~125 km relative to picture.)

rapidly deepening oceanic cyclones has been given by Sanders and Gyakum (1980). The authors suggest that failure to account for the influence of cumulus convection on large-scale circulations is mostly responsible for the more egregious underprediction errors in storm central pressure associated with operational NMC models over a wide range of grid meshes.

## 8. NMC LFM-II model forecasts

An inspection of selected 12, 24 and 48 h operational LFM-II forecasts verifying 1200 GMT shown in Fig. 19 discloses four major errors (compare against Figs. 1, 2 and 11). First, the model underforecasts the storm central pressure by an average of 8–16 mb. Second, the model fails to generate the observed strong surface pressure gradient to the west of the cyclone center. Third, the corresponding quantitative precipitation forecasts are woeful and, fourth, the offshore thermal ridge as defined by the thickness pattern is nearly absent. These errors persist in similar forecasts verifying 12 h later. The model tropospheric circulation forecasts, as typified by the 500 mb level on the other hand (not shown), are much better in defining both the phase, amplitude and vorticity structure of the short-wave trough that approaches the east coast. Viewed from the 25 year historical perspective of numerical weather prediction, the forecast must still be considered remarkable when one considers that as recently as 10–15 years ago, such a forecast could not have even been made. Deficient as the surface forecast is, it still alerts the forecaster that possible trouble could be in the offing for coastal residents.

Model failure to predict cyclogenesis in the conterminous United States and vicinity is a comparatively rare event. This section will concentrate on some possible physical explanations that might be relevant to the model forecast failure, ever mindful that numerical weather prediction is an extremely complex process and not often amenable to simple physical reasoning.

Fig. 20 represents a composite sea surface temperature analysis for the 18–20 February period based on all available ship and buoy data. The most

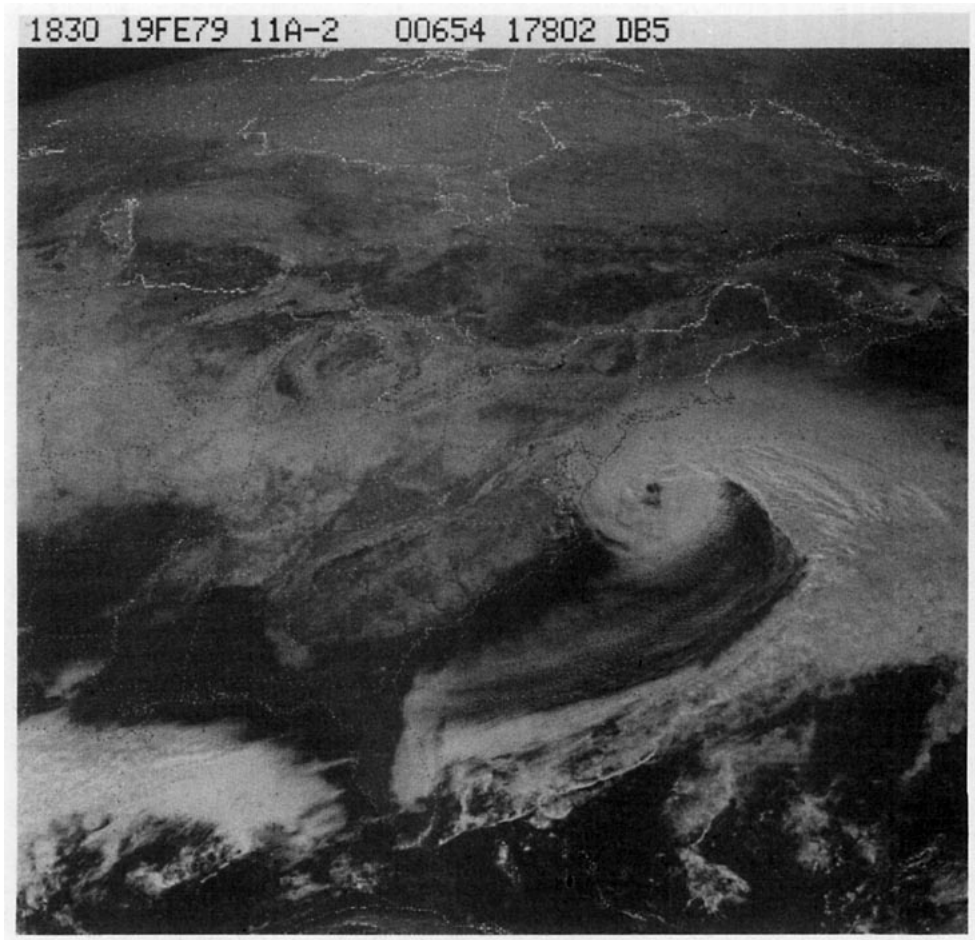


FIG. 16. As in Fig. 12 except for 1830 GMT 19 February 1979. (Misgridding: Shift geography southeastward ~50 km relative to picture.)

interesting feature is the tongue of very warm sea surface temperatures (SST) parallel to the coast and 200 km seaward in association with the Gulf Stream. Comparison of the observed sea surface temperature distribution with a long-term February climatology suggests an ~2°C increase in thermal contrast between nearshore and offshore waters during the time of cyclogenesis. In any case, the gradient of SST is rather large along the immediate coastal margins where cyclogenesis originated. Farther east the water is considerably cooler. Sanders and Gyakum (1980) find that explosive cyclogenesis occurs over a wide range of SST's, but particularly near the strongest gradients. In view of the extremely cold air overlying this warm water, oceanic sensible and latent heat fluxes might seem important to the establishment of a lower tropospheric baroclinic zone parallel to the coast along which preferential development can take place.

Sensible and latent heat fluxes are computed from the bulk aerodynamic formula at various times with the results for 0000 GMT 19 February shown in Fig. 21. At this time the computations are made along a line extending normal to the coast from Wilmington, North Carolina representing atmospheric conditions in advance of the cyclone. The drag coefficients for heat and water vapor are assumed equal to $1.6 \times 10^{-3}$ and values of temperature, specific humidity, wind speed and direction are taken from the detailed subjective analyses. A boundary layer 150 mb deep is used in order to convert the sensible heat flux into an equivalent boundary-layer heating rate on the basis of coastal sounding data.

For the 12 h period ending 0000 GMT 19 February, the latent heat flux is roughly double the sensible heat flux with the total flux averaging 600 W $m^{-2}$. On the average, the heat flux peaks 150–200 km offshore. The sensible heat flux implies a boundary layer warming of a little more than 10°C $day^{-1}$. A corresponding 12 h 1000–300 mb thickness change of 120 m arises if all of the latent heat flux is realized as condensation accompanying ascent and adiabatic cooling is ignored. This is unrealistic but serves as an upper bound estimate.

These heat fluxes are quite comparable to those reported by Petterssen *et al.* (1962) for various cat-

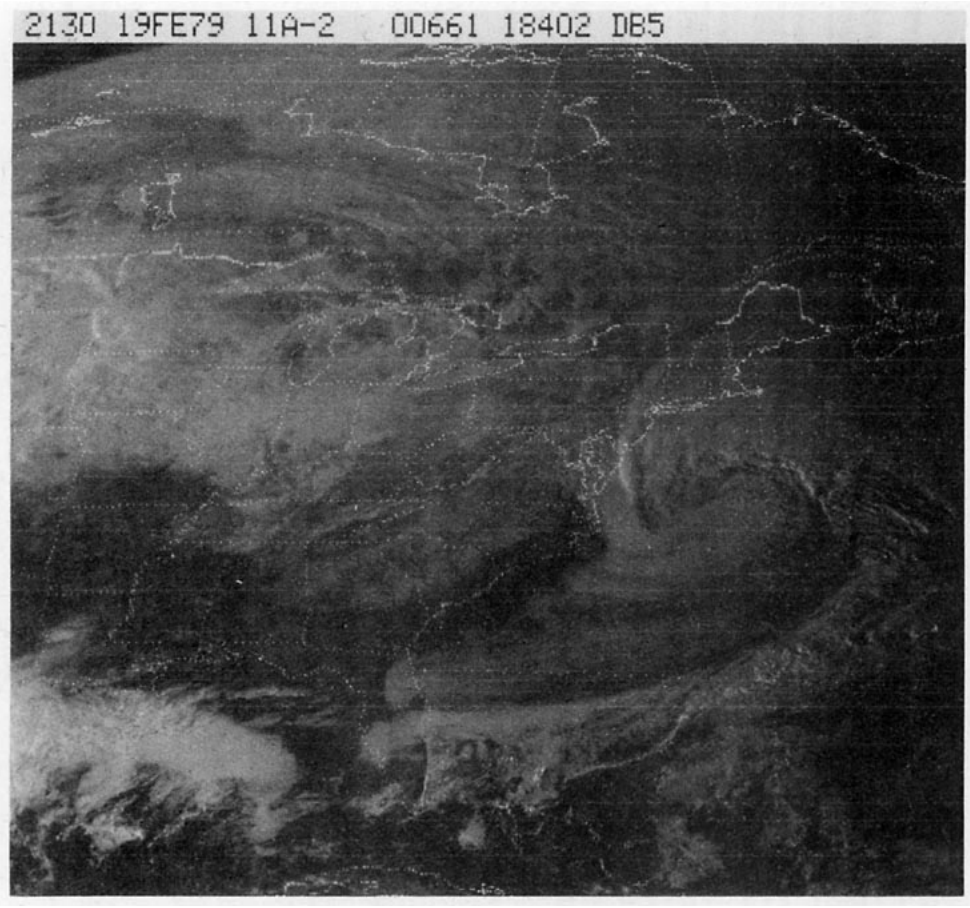


FIG. 17. As in Fig. 12 except for 2130 GMT 19 February 1979. (Misgridding: Shift geography westward ~100 km relative to picture.)

egories of Atlantic cyclones. A big difference, however, is that Petterssen *et al.* typically found the largest heat fluxes in the *wake* of a cyclone passage, whereas in the present case the large values are found in *advance* of the surface cyclone. These heat fluxes are continually sustained by a renewable supply of cold air provided by the strong anticyclone to the north. The net effect of offshore heating coupled with a cold surface flow inland is the reinforcement of a low-level baroclinic zone in advance of the developing cyclone and extending north-northeastward parallel to the coast. The importance of the lower tropospheric baroclinic zone in this case is that it apparently serves as a steering channel for shallow cyclogenesis by the means of the Laplacian of thermal advection. As a result the developing cyclone is steered to the *left* of the instantaneous 500 mb flow.

Meanwhile, the potent mid-tropospheric shortwave trough in the Ohio Valley is moving eastward toward the coast. By 1200 GMT 19 February the juxtaposition of the upper and lower tropospheric features has occurred in such a manner that an area of appreciable positive thermal vorticity advection overlies the surface cyclone center. Explosive development to a well-defined vortex structure then ensues. Apparently, the Presidents' Day cyclone event represents a case whereby a specific mesoscale circulation feature, i.e., the coastal front, has a significant impact on the evolution of the synoptic-scale flow pattern. The overall development is similar to that of type B cyclogenesis as described by Miller (1946). In this case, the coastal front seems to be an *extra* ingredient that causes the incipient cyclone to hug the coast. The coastal front in turn is reinforced by differential heating and moistening associated with the prevailing easterly geostrophic flow. This process is vigorous enough so that eventually the air feeding into the cyclone center can support convection whereupon explosive deepening ensues.

Currently, the operational LFM model parameterizes oceanic sensible heat flux but ignores the latent heat flux. The net result is that boundary-layer air is simultaneously warmed and dried accompanying a cold onshore flow above a warm sea surface as opposed to warming and moistening in the real atmosphere case. Previous researchers

(e.g., Winston, 1955; Pyke, 1965; Gall and Johnson, 1971), have commented on the tendency for explosive cyclogenesis to occur in regions of vigorous upward oceanic sensible and latent heat flux. The role of surface heating in cyclogenesis is controversial, however. Mansfield's (1974) theoretical work and the numerical investigation of Danard and Ellenton (1980) raise questions about its significance to development. Much of the controversy seems to arise from confusion in terminology. The surface heating in this case does not cause cyclogenesis. Rather it helps to establish a favorable low-level baroclinic zone on which development can then take place in response to an external forcing mechanism. The normal situation, however, is for the heat flux to be dominant with the flow of cold continental air offshore across progressively warmer ocean temperatures. The present situation is somewhat unique in that the fluxes are strong but the flow direction is reversed, i.e., it is onshore. Ballentine's (1980) numerical results show the importance of the surface heat flux to the ultimate intensity of the coastal front. The differential diabatic heating term has not been computed in the frontogenesis equation (2) due to uncertainties in specifying the diabatic heating rate. Based on a comparison, however, of this case and Ballentine's, it would be surprising if the effect did not turn out to be frontogenetical. According to Dr. Dennis Deaven (private communication), a slight improvement resulted in the surface pressure pattern near the cyclone center in this case in a special research run of the LFM-II at NMC which incorporated oceanic latent heat flux. Obviously, the LFM-II is not intended to capture the details of the coastal front circulation.

An examination of the initial model boundary layer (lowest 50 mb) structure and comparison with observation is revealing. From the plotted soundings, an average boundary layer potential temperature is derived for the lowest 50 mb above the ground at each radiosonde station. Adjacent oceanic values are derived from the reported ship observations coupled with reconstructed lapse rates on both sides of the coastal front. These values are then subjectively analyzed and tabulated at LFM grid points from initial analyses kindly provided by NMC.

Fig. 22 shows the observed planetary boundary layer (PBL) potential temperature structure for all three time periods superimposed on the difference field between the initial LFM-II analysis and observed field. In this figure a positive (negative) difference field corresponds to an initial model boundary layer that is too warm (cold). The results are rather striking in showing that the model initial state underestimates the boundary-layer baroclinicity parallel to the coast. The model initial state is

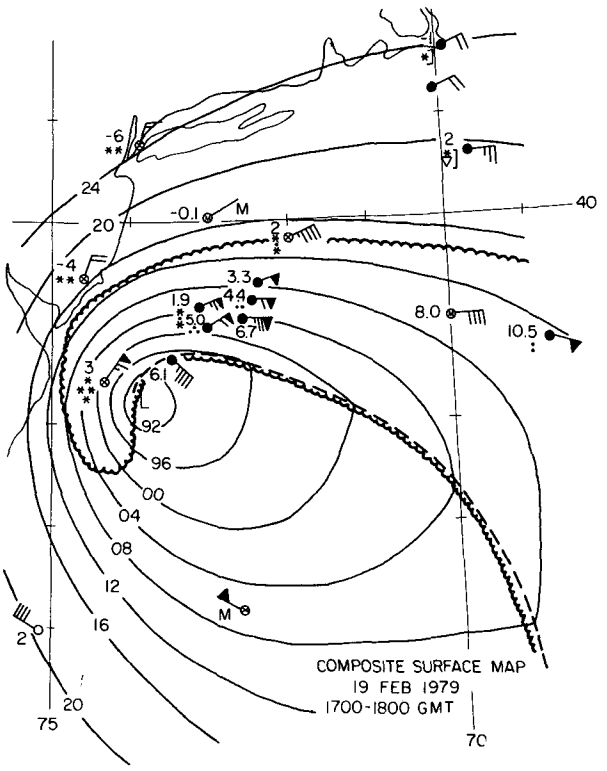


FIG. 18. Composite surface sectional map for 1700–1800 GMT 19 February 1979. Winds in m $s^{-1}$ as per Fig. 1 plotting convention, isobars in mb, temperatures in °C with conventional plotting and analysis. Escolloped lines enclose convective region shown in Fig. 16.

clearly deficient in defining the magnitude of the boundary-layer cold dome between the Appalachians and the coast. Similarly, the model initial state does not do justice to the warm air just off the coast. The latter problem is particularly severe at 1200 GMT 19 February with the boundary layer 8–12°C too cold in the vicinity of the cyclone center. This would certainly have to exert a damping effect on any model parameterized convective processes.

A possible partial cause of the apparent boundary-layer analysis deficiency in the present case might be the absence of significant level sounding data in the initial analysis cycle. The model boundary-layer potential temperature is derived from a vertical interpolation of the 850 mb and surface temperature analyses. This procedure can lead to an erroneous boundary-layer potential temperature when a strong inversion with base below 850 mb exists such as in the present case. Viewed in another way, consider Figs. 23 and 24 which give kinematic omega profiles for various triangles at the indicated times. The computation procedure is identical to before except 200 mb was used for the upper boundary. Observe the south-to-north increase in the height of the level of maximum ascent at 1200 GMT. In all cases, however, the maximum

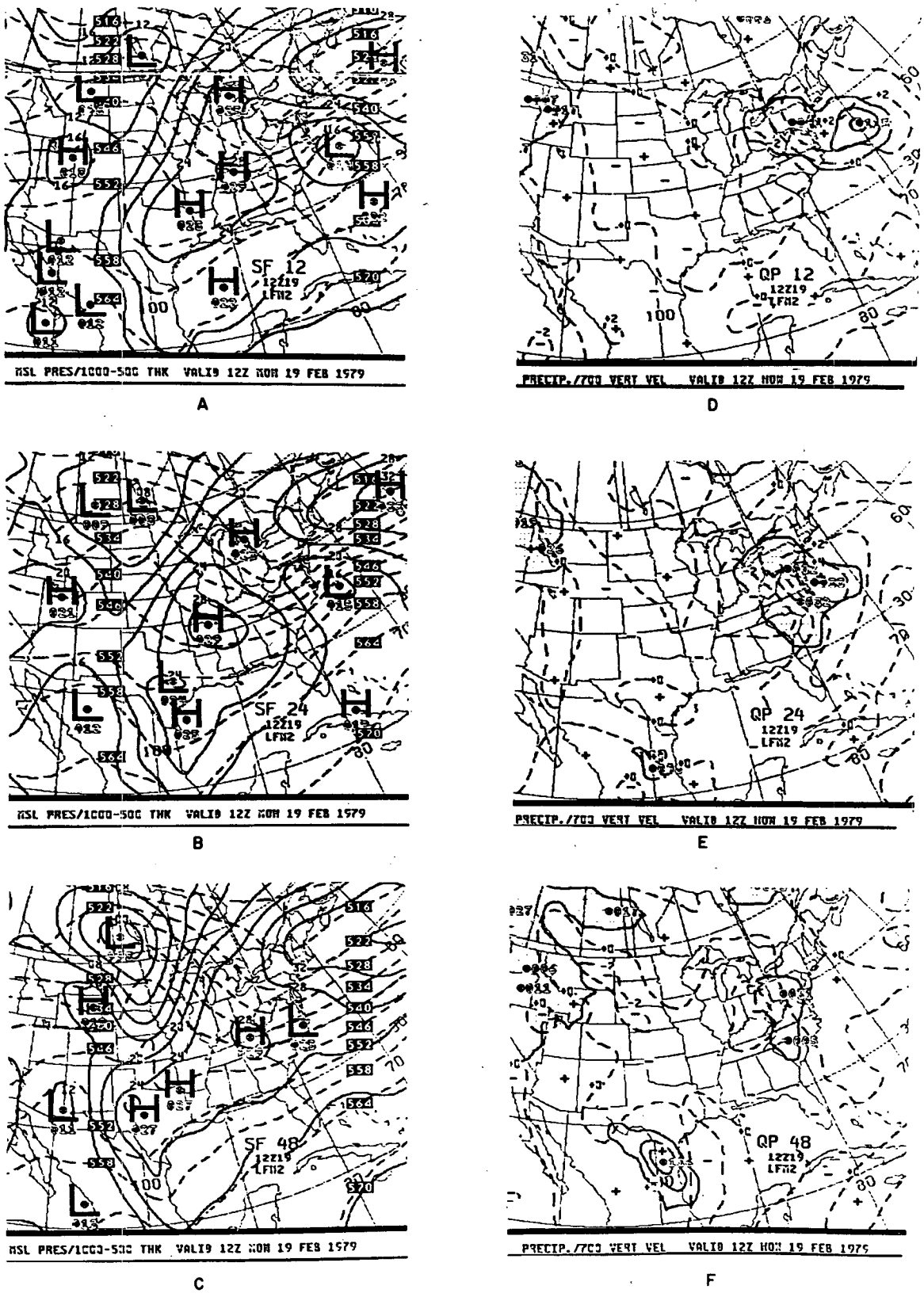


FIG. 19. Operational NMC LFM-II 12 h (A), 24 h (B) and 48 h (C) mean sea level pressure (solid lines, mb) and 1000–500 mb thickness (dashed lines, dam) prognoses valid 1200 GMT 19 February 1979; similarly for 12 h (D), 24 h (E) and 48 h (F) 700 mb vertical motion (dashed lines, $\omega \times 10^{-3}$ mb $s^{-1}$) and accumulated 12 h precipitation (solid lines, hundredths of an inch). Precipitation contours at 0.01 inch (0.25 mm), 0.50 inch (12.5 mm) and 1.00 inch (25.0 mm).

ascent is found in the lower troposphere. In particular, the triangles bracketing the coastal front (AYS–CHS–AHN and COF–AYS–AQQ) show the level of maximum ascent between 750 and 850 mb. A relatively low ascent level is still seen at 0000 GMT despite an overall increase in the vigor of the vertical motions. Likewise a low maximum ascent level was observed at 1200 GMT 19 February in the storm environment (Fig. 14).

Consequently, experiments designed to test the effect of increased vertical resolution in the model lower troposphere *together* with the use of mandatory *and* significant level sounding data might be fruitful for classes of storms in which a strongly baroclinic boundary layer appears essential to understanding the overall dynamics. Indeed, Anthes and Keyser (1979) have shown how variations in PBL structure can exert a significant impact on short-range forecasts of cyclogenesis while Anthes *et al.* (1980) showed the importance of proper PBL resolution in a numerical model for realistic forecasts in cases of differentially heated baroclinic boundary layers. Current model horizontal resolution would seem adequate to capture the cold air dammed up east of the Appalachians and the essense of the coastal zone baroclinicity. Many interesting mesoscale phenomena seem to develop along the edges or boundaries of synoptic-scale systems as defined by temperature and moisture gradients which may be topographical or geographical in origin. Provided the synoptic-scale circulation forecast is reasonable, then adequate horizontal and vertical resolution of these boundaries from the initial analysis cycle onward should at least force the large-scale forecast in the right direction even though an explicit representation of the particular mesoscale circulation may not be possible.

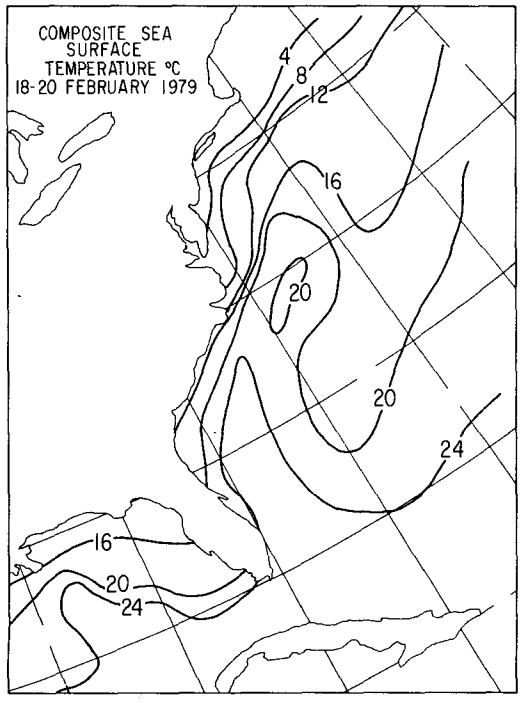


FIG. 20. Composite sea surface temperature analysis (°C) for the period 18–20 February 1979.

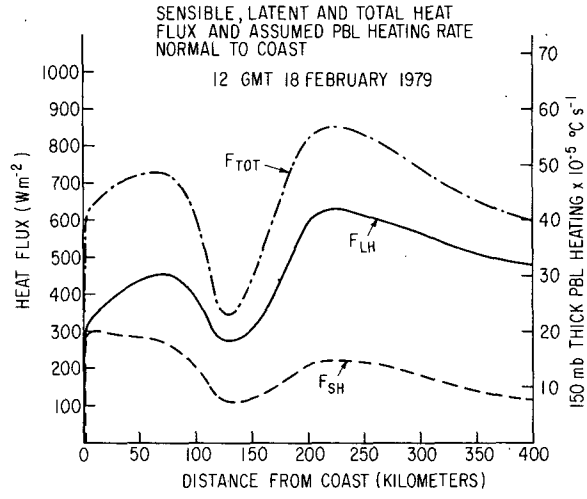


FIG. 21. Sensible ($F_{SH}$), latent ($F_{LH}$) and total heat flux ($F_{TOT}$) in W m$^{-2}$ and corresponding PBL sensible heating rate in $10^{-5}$ °C s$^{-1}$ for an assumed 150 mb thick PBL for 0000 GMT 19 February 1979.

Finally, the importance of convection in this case suggests consideration of model cumulus parameterization schemes. Anthes and Keyser (1979) show that the surface pressure evolution in a fine-mesh model is rather sensitive to the choice of cumulus parameterization scheme and the resulting vertical distribution of latent heat release. At the time of the Presidents' Day storm the operational LFM-II employed a simplified moist convective adjustment procedure as described by Gerrity (1977)[4] for this purpose. Failure to account properly for the convective precipitation in the moisture conservation equation and the first law of thermodynamics resulted in overly generous quantitative precipitation forecasts in the vicinity of active frontal zones and accompanying cold air outbreaks to the detriment of forecast skill as shown by Bosart (1980).

Subsequent to the President's Day cyclone, the operational LFM-II moist convective procedure was changed to give a grid-column moisture convergence type of scheme similar to that employed in many current numerical models. At Albany and Boston, LFM-II quantitative precipitation skill scores have improved since this implementation in daily forecasting using the methods described by Sanders (1979). A re-run of the LFM-II for this case using the modified convective scheme (Dr. Dennis Deaven, private communication) resulted in slight improvements in the sea level pressure pattern

[4] Gerrity, J. F., Jr., 1977: The LFM model—1976: A documentation. National Oceanographic and Atmospheric Administration, Tech. Memo. NWS-NMC-60, 67 pp. [NTIS PB 279-419].

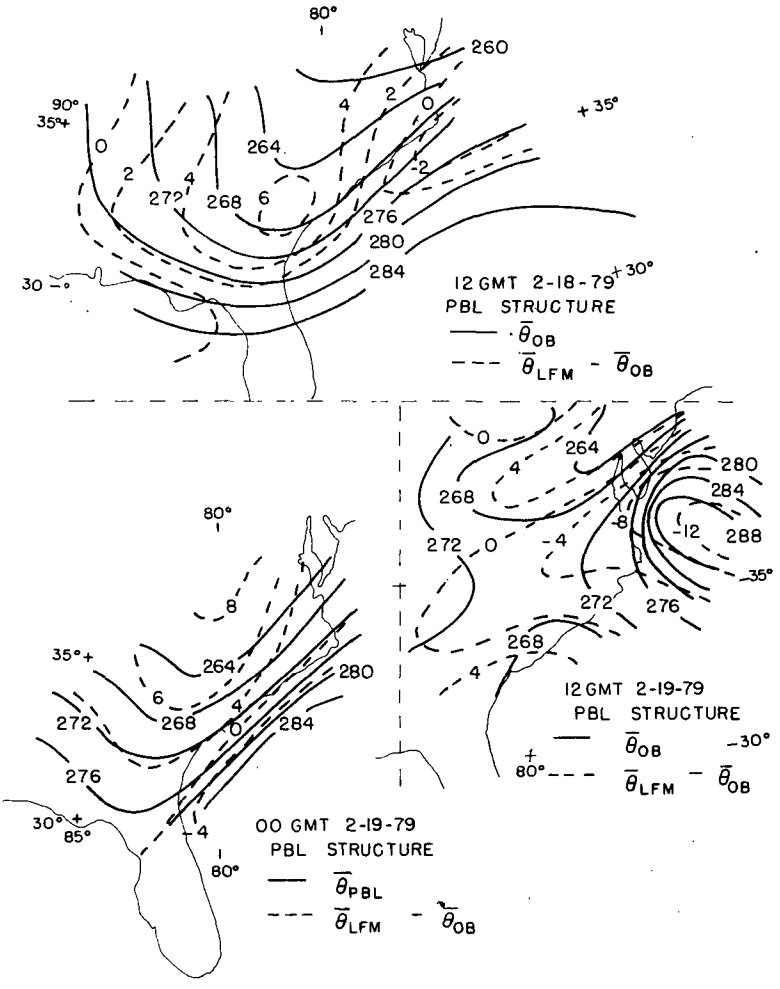


FIG. 22. Observed PBL potential temperature (K, solid lines) structure (lowest 50 mb) based on mandatory and significant level sounding data. The difference field (°C) is obtained by subtracting this analysis from the LFM-II initial analysis is given by the dashed lines.

prognoses and modest improvements in the rainfall forecasts. These changes, although in the correct direction, did not significantly alter the four major model errors mentioned previously. Perhaps the unduly cold oceanic model boundary layer exerted a damping effect on model convection.

## 9. Discussion

Recently, Reed (1979) and Rasmussen (1979) have debated the possible dynamics relative to the development of small-scale disturbances such as polar lows. The argument centers around whether polar lows should be considered creatures of baroclinic instability or forced by convective processes analogous to tropical disturbances (CISK) as originally discussed by Charney and Eliassen (1964). While it seems likely that the Presidents' Day cyclone originated as a baroclinic disturbance aided in a significant way by differential diabatic heating, the possible importance of CISK to the continuing development of the cyclone cannot be ruled out. Reed favors the polar low as a baroclinic disturbance but he points out that CISK influences cannot be ruled out unless it can be convincingly established that the organization of convection does not in turn feed back to intensify the larger scale system. Additional support for these ideas comes from the work of Mullen (1979) and he also suggests that the possible role of nonlinear wave interaction needs to be researched carefully before concluding that condensational heating and small static stability are necessary for the formation of such disturbances.

In the present case, cumulus convection rapidly developed near the cyclone center preceding and accompanying the generation of an intense vortex with a hurricane-eye-like structure. The strongest

surface winds are concentrated in the northern semicircle of the storm where the cold anticyclone to the north is apparently able to continually sustain superadiabatic lapse rates near the warm ocean surface. Perhaps this process in turn acts to continue to feed the developing cumulus convection while maintaining the horizontal temperature gradient. As with hurricanes, the low roughness lengths over water may be crucial in the development of a positive feedback.

Coastal front initiated cyclogenesis differs from polar low development in terms of the presence of a very strong baroclinic boundary layer at the initial time. The potential for cyclogenesis in the presence of a horizontal temperature gradient adjacent to a rigid boundary has been discussed from a theoretical point of view by Charney and Stern (1962). Staley and Gall (1977) have used a four-layer quasi-geostrophic model to show that the wavelength of maximum instability can be shortened from 4000 to 2000 km when the lower troposphere is significantly baroclinic and static stability is small, conditions that are satisfied in the present case. Blumen (1979) has essentially confirmed Staley and Gall's (1977) findings by means of a linearized two-layer Eady model. Additionally, Blumen (1979) has pointed out that the growth rate accompanying short-wave baroclinic instability is rather sensitive to the thickness of the model layers. He suggests that it may be necessary to consider models with greater vertical resolution in order to produce reasonably continuous static stability variations germane to short wave baroclinic instability.

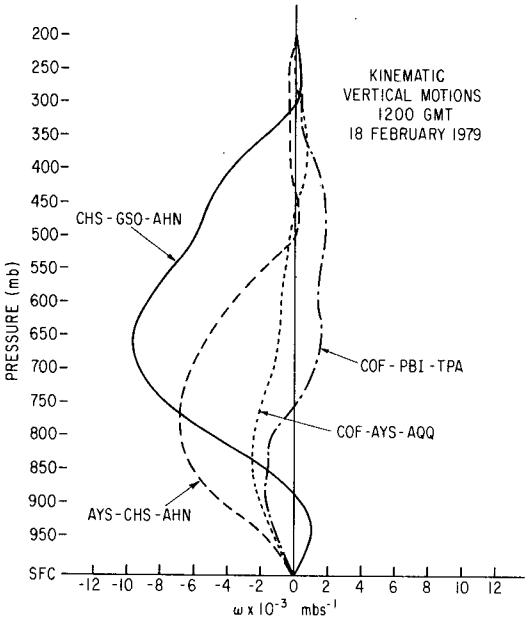


FIG. 23. Kinematic vertical motion profiles ($\times 10^{-3}$ mb $s^{-1}$) for triangles defined by the indicated radiosonde stations. See Fig. 25 and the Appendix for station information. All times 1200 GMT 18 February 1979.

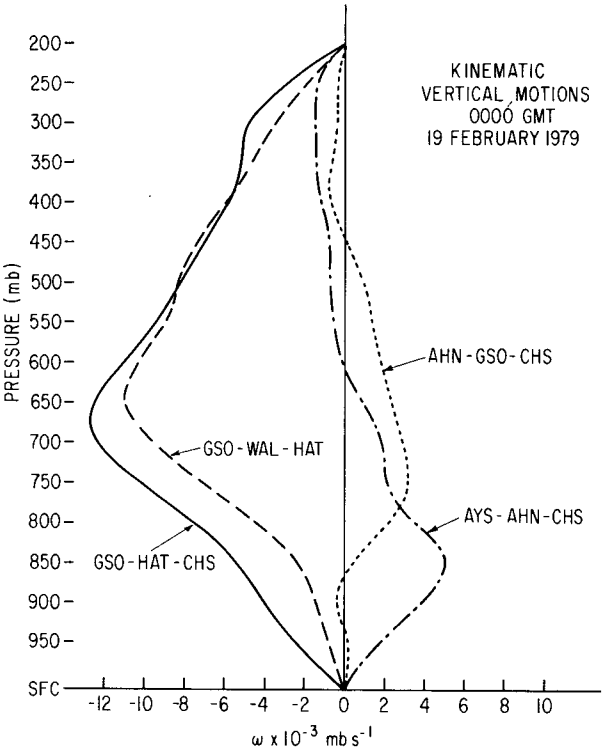


FIG. 24. As in Fig. 23 except for 0000 GMT 19 February 1979.

Uccellini *et al.* (1981), using arguments contained in Uccellini and Johnson (1979) and Uccellini (1980) together with additional evidence, have suggested that the pronounced ageostrophic circulation seen on the 850 mb surface at 1200 GMT February (Fig. 1a) may be a manifestation of the lower branch of a forced, thermally indirect circulation embedded in the exit region of a propagating jet streak system in the subtropical jet stream. They view the jet streak forcing as essential to the developmental process with a significant modifying effect provided by cold air damming east of the Appalachians. The present paper, in contrast, favors boundary-layer and convective-scale forcing as the fundamental physical mechanisms leading to the explosive cyclogenesis. Further diagnostic and prognostic research should be useful in resolving some of these questions.

Finally, from a forecasting point of view, one valuable lesson of the partially unforeseen cyclone development is that the forecaster should be especially alert when the southwest quadrant of an anticyclone is forecast to come under the influence of a major short-wave trough in the presence of a strongly baroclinic boundary layer forced by diabatic heating. If this atmosphere in turn has a tendency to become conditionally unstable then explo-

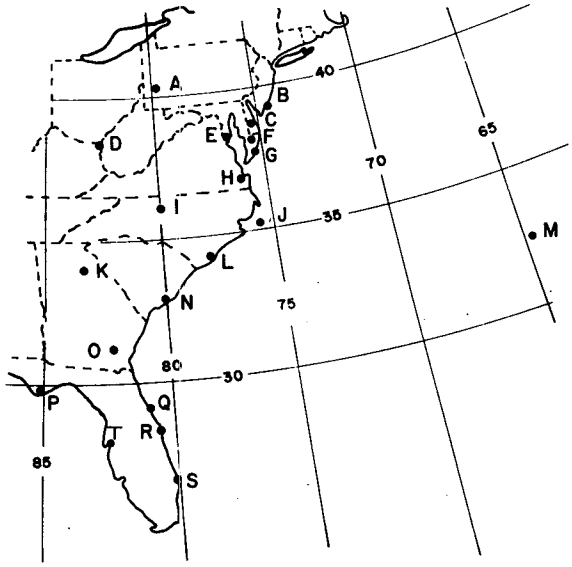


FIG. 25. Geographical locator map: A, Pittsburgh, PA; B, Atlantic City, NJ; C, Dover, DE; D, Huntington, WV; E, Patuxent River, MD; F, Salisbury, MD; G, Wallops Island, VA; H, Norfolk, VA; I, Greensboro, NC; J, Cape Hatteras, NC; K, Athens, Ga; L, Wilmington, NC; M, Bermuda; N, Charleston, SC; O, Waycross, Ga; P, Apalachicola, FL; Q, Daytona Beach, FL; R, Cape Canaveral, FL; S, West Palm Beach, FL; and T, Tampa, FL.

sive cyclogenesis on a relatively small scale may result.

Additionally, there is often a wealth of useful meteorological information that for one reason or another is not available to the operational forecast system. In the present case, valuable analysis information was obtained from ships logs provided by the National Climatic Center and not available in real time to NMC, as well as ship data that were slightly delayed and of no use to the LFM forecast cycle but of considerable use to forecasters.

## 10. Conclusions

Prior to the record-breaking snowstorm of 18–19 February 1979 in the Middle Atlantic States, a massive, cold Canadian anticyclone invades the eastern United States. A well-defined baroclinic zone in the lower half of the troposphere extends from Texas eastward to the western Atlantic Ocean. Within this broad baroclinic zone, a region of enchanced baroclinicity forms in the lower troposphere along the Carolina coast accompanying the onshore flow of cold continental air south of the anticyclone. The cold air is rapidly warmed and moistened by oceanic sensible and latent heat fluxes, leading to the creation of a highly baroclinic boundary layer superimposed over a region of strong, horizontal sea surface temperature gradient.

Quasi-geostrophic lower tropospheric warm advection and, to a lesser extent, middle tropospheric differential cyclonic vorticity advection trigger ascent, low-level convergence and surface pressure falls along the coastal front. The resulting growth in vertical circulation is produced by an as yet unknown combination of external forcing from a weak southern extension of a migratory short-wave trough and/or a propagating upper tropospheric jet-streak system. This leads to the growth of a shallow cyclone which continually develops north-northeastward parallel to the coast and steered by the instantaneous low-level flow. Simultaneously, a vigorous mid-tropospheric short wave located east of the Mississippi River Valley moves eastward toward the Atlantic coast. The shallow cyclone east of the Carolinas would probably have remained innocuous were it not for the fact that it moves to the *left* of the instantaneous mid-tropospheric flow. The resulting coastal storm track allows the cyclone to eventually come under the favorable positive thermal vorticity advection region of the eastward propagating short-wave trough. A specific example of the influence of a mesoscale feature on the evolution of a synoptic-scale circulation feature is thus suggested.

Rapid cyclone deepening begins in the early morning hours of 19 February in the vicinity of Cape Hatteras, North Carolina. The deepening is in accord with quasi-geostrophic theory but the rapidity is not. Simultaneous with the onset of deepening, convection is observed to break out near and to the east of the incipient storm center where cold polar air is rapidly being warmed, moistened and destabilized by oceanic sensible and latent heat fluxes. Explosive deepening and transformation of the cyclone to a vortex with hurricane-like characteristics in the form of a closed eye, and hurricane-force surface winds coincide with the outbreak of this convection. Unlike a hurricane, however, the distribution of convection is very asymmetric, being primarily concentrated to the north and east of the vortex in the region of strongest surface winds.

The evolution of the cyclone is poorly handled by the operational NMC LFM-II model. The major errors involve the failure of the model to capture the intensity of the sea level pressure pattern and resulting quantitative precipitation distribution. A number of possible reasons are advanced for the model failure including inadequate vertical resolution, omission of significant level sounding data from the initial analysis cycle, improper boundary-layer physics, and the inability to simulate the bulk effects of convective-scale processes adequately.

The isolation of these errors in conjunction with the physical understanding derived from a detailed analysis of the President's Day cyclone provides an attractive framework for testing a number of sci-

entific hypotheses in that cyclones characterized by strong boundary-layer and convective-scale forcing represent situations designed to exert maximum stress on existing research and operational prediction models. Finally, the results lend further weight to recent evidence that failure to model the bulk effects of convective-scale processes and oceanic heat and moisture fluxes properly is a significant stumbling block to progress in correctly simulating oceanic cyclogenesis.

*Acknowledgments*. This work was initiated while the author was on sabbatical leave at MIT for the 1978–79 academic year. I am grateful to Professor Fred Sanders, John Gyakum and other members of the MIT Convection Club for many stimulating discussions about this case.

I also appreciate the comments of Rodney Gonski of the National Weather Service Forecast Office in Raleigh, North Carolina and Louis Uccellini of NASA-Goddard for alerting me to the possible role of an upper tropospheric jet streak circulation in inducing low-level warm advection over the coastal front.

I thank Louis Uccellini, John Gyakum and Roger Pielke for a thorough review of the manuscript and continuing interest in this work. The referees made helpful comments for tightening the original manuscript.

I extend thanks to participants in the East Coast Rig Instrumentation Program (CONOCO, Exxon, Gulf, Houston Oil and Minerals, Mobil, Shell and Texaco) for providing me with drilling rig meteorological data from the Baltimore Canyon area which was crucial in pinning down the ultimate intensity of the offshore cyclone.

NCAR provided much of the upper air data for this study. Tony Tancreto, former meteorologist-in-charge, National Weather Service Forecast Office, Boston, provided valuable teletype data that otherwise would have been lost. Thanks to Vito Pagnotti for assistance in performing the frontogenesis and quasi-geostrophic omega calculations. The figures were drafted by Ms. Isabel Kole of MIT and Mrs. Marilyn Peacock of SUNYA. The manuscript was typed by Ms. Sally Young. Research support was provided through National Science Foundation Grants g78-15942-ATM (MIT) and ATM 7800531 (SUNYA).

## APPENDIX

**Weather Station Identifiers for Locations Given in Fig. 25**

| Station | International identifier | U.S. identifier | Latitude (°N) | Longitude (°W) | Elevation (m) |
|---|---|---|---|---|---|
| West Palm Beach, FL | 72203 | PBI | 26.7 | 80.1 | 6 |
| Cape Canaveral, FL | 74794 | COF | 28.5 | 80.5 | 2 |
| Daytona Beach, FL | — | DAB | 29.2 | 81.0 | 12 |
| Tampa, FL | 72211 | TPA | 28.0 | 82.5 | 6 |
| Apalachicola, FL | 72220 | AQQ | 29.7 | 85.0 | 12 |
| Charleston, SC | 72208 | CHS | 32.9 | 80.0 | 15 |
| Bermuda | 78016 | HKD | 32.3 | 64.7 | 6 |
| Wilmington, NC | 72301 | ILM | 34.3 | 77.9 | 11 |
| Waycross, GA | 72213 | AYS | 31.3 | 82.4 | 43 |
| Athens, GA | 72311 | AHN | 33.9 | 83.2 | 247 |
| Cape Hatteras, NC | 72304 | HAT | 35.3 | 80.9 | 3 |
| Greensboro, NC | 72317 | GSO | 36.1 | 79.9 | 270 |
| Norfolk, VA | 72308 | ORF | 36.9 | 76.2 | 9 |
| Wallops Island, VA | 72402 | WAL | 37.9 | 75.5 | 15 |
| Salisbury, MD | — | SBY | 38.3 | 75.5 | 17 |
| Patuxent River, MD | 72404 | NHK | 38.3 | 76.4 | 14 |
| Huntington, WV | 72425 | HTS | 38.3 | 82.5 | 255 |
| Dover, DE | — | DOV | 39.3 | 75.5 | 12 |
| Atlantic City, NJ | 72407 | ACY | 39.5 | 74.6 | 20 |
| Pittsburgh, PA | 72520 | PIT | 40.5 | 80.2 | 373 |

## REFERENCES

Anthes, R. A., and D. Keyser, 1979: Tests of a fine-mesh model over Europe and the United States. *Mon. Wea. Rev.*, **107**, 963–984.

——, N. L. Seaman and T. T. Warner, 1980: Comparisons of numerical simulations of the planetary boundary layer by a mixed-layer and a multi-level model. *Mon. Wea. Rev.*, **108**, 365–376.

Baker, D. G., 1970: A study of high pressure ridges to the east of the Appalachian mountains. Ph.D. dissertation, Massachusetts Institute of Technology, 127 pp.

Ballentine, R. J., 1980: A numerical investigation of New England coastal frontogenesis. *Mon. Wea. Rev.*, **108**, 1479–1497.

Bergeron, T., 1949: The problem of artificial control of rainfall on the globe. II. The coastal orographic maxima of precipitation in autumn and winter. *Tellus*, **1**, 15–32.

Blumen, W., 1979: On short-wave baroclinic instability. *J. Atmos. Sci.*, **36**, 1925–1933.

Bosart, L. F., 1975: New England coastal frontogenesis. *Quart. J. Roy. Meteor. Soc.*, **101**, 957–978.

——, 1980: Evaluation of LFM-2 quantitative precipitation forecasts. *Mon. Wea. Rev.*, **108**, 1087–1099.

——, C. J. Vaudo and J. H. Helsdon, Jr., 1972: Coastal frontogenesis. *J. Appl. Meteor.*, **11**, 1236–1258.

Brown, H. E., and D. A. Olson, 1978: Performance of NMC in forecasting a record-breaking winter storm 6–7 February 1978. *Bull. Amer. Meteor. Soc.*, **59**, 562–575.

Charney, J. G., and A. Eliassen, 1964: On the growth of the hurricane depression. *J. Atmos. Sci.*, **21**, 68–75.

——, and M. E. Stern, 1962: On the stability of internal baroclinic jets in a rotating atmosphere. *J. Atmos. Sci.*, **19**, 159–172.

Danard, M. B., and G. E. Ellenton, 1980: Physical influences on east coast cyclogenesis. *Atmos.-Ocean*, **18**, 65–82.

Dickson, R. R., 1979: Weather and circulation of February 1979: Near record cold of the northeast quarter of the country. *Mon. Wea. Rev.*, **107**, 624–630.

Eliassen, A., 1962: On the vertical circulation in frontal zones. *Geofys. Publ.*, **24**, 147–160.

Gall, R. L., and D. R. Johnson, 1971: The generation of available potential energy by sensible heating: A case study. *Tellus*, **21**, 465–482.

Herzegh, P. H., and P. V. Hobbs, 1980: The mesoscale and microscale structure and organization of clouds and precipitation in midlatitude cyclones. II: Warm-frontal clouds. *J. Atmos. Sci.*, **37**, 597–611.

Hobbs, P. V., T. J. Matejka, P. H. Herzegh, J. D. Locatelli and R. A. Houze, Jr., 1980: The mesoscale and microscale structure and organization of clouds and precipitation in midlatitude cyclones. I: A case study of a cold front. *J. Atmos. Sci.*, **37**, 568–596.

Mansfield, D. A., 1974: Polar lows: the development of baroclinic disturbances in cold air outbreaks. *Quart. J. Roy. Meteor. Soc.*, **100**, 541–554.

Marks, F. D., and P. M. Austin, 1979: Effects of the New England coastal front on the distribution of precipitation. *Mon. Wea. Rev.*, **107**, 53–67.

Miller, J. E., 1946: Cyclogenesis in the Atlantic coast region of the United States. *J. Meteor.*, **3**, 31–44.

Mullen, S. L., 1979: An investigation of small synoptic scale cyclones in polar air streams. *Mon. Wea. Rev.*, **107**, 1636–1647.

O'Brien, J. J., 1970: Alternative solutions to the classical vertical velocity problem. *J. Appl. Meteor.*, **9**, 197–203.

Petterssen, S., D. L. Bradbury and K. Pedersen, 1962: The Norwegian cyclone models in relation to heat and cold sources. *Geofys. Publ.*, **24**, 243–280.

Pyke, C. B., 1965: On the role of air-sea interaction in the development of cyclones. *Bull. Amer. Meteor. Soc.*, **46**, 4–15.

Rasmussen, E., 1979: The polar low as an extratropical CISK disturbance. *Quart. J. Roy. Meteor. Soc.*, **105**, 531–549.

Reed, R. J., 1977: The development and status of modern weather prediction. *Bull. Amer. Meteor. Soc.*, **58**, 390–400.

——, 1979: Cyclogenesis in polar air streams. *Mon. Wea. Rev.*, **107**, 38–52.

Sanders, F., 1955: An investigation of the structure and dynamics of an intense surface frontal zone. *J. Meteor.*, **12**, 542–552.

——, 1971: Analytic solutions of the nonlinear omega and vorticity equation for a structurally simple model of disturbance in the baroclinic westerlies. *Mon. Wea. Rev.*, **99**, 393–407.

——, 1979: Trends in skill of daily forecasts of temperature and precipitation, 1966–1978. *Bull. Amer. Meteor. Soc.*, **60**, 763–769.

——, and J. R. Gyakum, 1980: Synoptic dynamic climatology of the bomb. *Mon. Wea. Rev.*, **108**, 1589–1606.

Sawyer, J. S., 1956: The vertical circulation at meteorological fronts and its relation to frontogenesis. *Proc. Roy. Soc. London*, **A234**, 346–362.

Spar, J., 1956: An analysis of a cyclone on a small synoptic scale. *Mon. Wea. Rev.*, **84**, 291–299.

Staley, D. O., and R. L. Gall, 1977: On the wavelength of maximum baroclinic instability. *J. Atmos. Sci.*, **34**, 1679–1688.

Tracton, M. S., 1973: The role of cumulus convection in the development of extratropical cyclones. *Mon. Wea. Rev.*, **101**, 573–593.

Uccellini, L. F., 1980: On the role of upper tropospheric jet streaks and leeside cyclogenesis in the development of low-level jets in the Great Plains. *Mon. Wea. Rev.*, **108**, 1689–1696.

——, and D. R. Johnson, 1979: The coupling of upper and lower tropospheric jet streaks and implications for the development of severe convective storms. *Mon. Wea. Rev.*, **107**, 682–703.

——, P. J. Kocin and C. H. Wash, 1981: The Presidents' Day cyclone 17–19 February 1979: An analysis of jet streak interactions prior to cyclogenesis. NASA Tech. Memo. 82077, 59 pp. [NTIS N81-20658].

Wagner, A. J., 1979: Weather and Circulation of January 1979—Widespread record cold and heavy snowfall in the Midwest. *Mon. Wea. Rev.*, **107**, 499–506.

Winston, J. S., 1955: Physical aspects of rapid cyclogenesis in the Gulf of Alaska. *Tellus*, **7**, 481–500.